REPORT DOCUMENTATION PAGE

Form Approved OMB NO. 0704-0188

The public reporting burden for this collection of information is estimated to average 1 hour per response, including the time for reviewing instructions, searching existing data sources, gathering and maintaining the data needed, and completing and reviewing the collection of information. Send comments regarding this burden estimate or any other aspect of this collection of information, including suggesstions for reducing this burden, to Washington Headquarters Services, Directorate for Information Operations and Reports, 1215 Jefferson Davis Highway, Suite 1204, Arlington VA, 22202-4302. Respondents should be aware that notwithstanding any other provision of law, no person shall be subject to any oenalty for failing to comply with a collection of information if it does not display a currently valid OMB control number.
PLEASE DO NOT RETURN YOUR FORM TO THE ABOVE ADDRESS.

1. REPORT DATE (DD-MM-YYYY)	2. REPORT TYPE	3. DATES COVERED (From - To)
06-02-2017	Final Report	1-Oct-2013 - 30-Sep-2016

4. TITLE AND SUBTITLE
Final Report: Continuous/Discontinuous Variational Multiscale Methods for Variable Density Flows

5a. CONTRACT NUMBER
W911NF-13-1-0452

5b. GRANT NUMBER

5c. PROGRAM ELEMENT NUMBER

6. AUTHORS
Guglielmo Scovazzi (PI)

5d. PROJECT NUMBER

5e. TASK NUMBER

5f. WORK UNIT NUMBER

7. PERFORMING ORGANIZATION NAMES AND ADDRESSES
Duke University
C/O Office of Research Support
2200 W. Main St., Ste. 710
Durham, NC 27705 -4677

8. PERFORMING ORGANIZATION REPORT NUMBER

9. SPONSORING/MONITORING AGENCY NAME(S) AND ADDRESS (ES)
U.S. Army Research Office
P.O. Box 12211
Research Triangle Park, NC 27709-2211

10. SPONSOR/MONITOR'S ACRONYM(S)
ARO

11. SPONSOR/MONITOR'S REPORT NUMBER(S)
64429-MA.2

12. DISTRIBUTION AVAILIBILITY STATEMENT
Approved for Public Release; Distribution Unlimited

13. SUPPLEMENTARY NOTES
The views, opinions and/or findings contained in this report are those of the author(s) and should not contrued as an official Department of the Army position, policy or decision, unless so designated by other documentation.

14. ABSTRACT
The discontinuous Galerkin (DG) method has found widespread application in elliptic problems with rough coefficients, of which the Darcy flow equations are a prototypical example. One of the long-standing issues of DG approximations is the overall computational cost, and many different strategies have been proposed: the variational multiscale DG method, the hybridizable DG method, the multiscale DG method, the embedded DG method, and the Enriched Galerkin method. We developed a new mixed method, which we named dual-scale Galerkin DG method (DSDG). In the DSDG method, the degrees of freedom of a less computationally expensive coarse scale

15. SUBJECT TERMS
Discontinuous Galerkin method; variational multiscale method; hybridization; elliptic problems; Darcy flow.

16. SECURITY CLASSIFICATION OF:			17. LIMITATION OF ABSTRACT	15. NUMBER OF PAGES	19a. NAME OF RESPONSIBLE PERSON
a. REPORT	b. ABSTRACT	c. THIS PAGE			Guglielmo Scovazzi
UU	UU	UU	UU		19b. TELEPHONE NUMBER 919-660-5075

Report Title

Final Report: Continuous/Discontinuous Variational Multiscale Methods for Variable Density Flows

ABSTRACT

The discontinuous Galerkin (DG) method has found widespread application in elliptic problems with rough coefficients, of which the Darcy flow equations are a prototypical example. One of the long-standing issues of DG approximations is the overall computational cost, and many different strategies have been proposed: the variational multiscale DG method, the hybridizable DG method, the multiscale DG method, the embedded DG method, and the Enriched Galerkin method. We developed a new mixed method, which we named dual-scale Galerkin DG method (DSDG). In the DSDG method, the degrees-of-freedom of a less computationally expensive coarse-scale approximation are linked to the degrees-of-freedom of a base DG approximation. The proposed approach has always similar or improved accuracy with respect to the base DG method, with a considerable reduction in computational cost. We completed an analysis of stability and convergence of the proposed method, in addition to a study on its conservation and consistency properties. Computational tests have confirmed the quality of the DSDG strategy.

Enter List of papers submitted or published that acknowledge ARO support from the start of the project to the date of this printing. List the papers, including journal references, in the following categories:

(a) Papers published in peer-reviewed journals (N/A for none)

Received		Paper
02/05/2017	1	Guoyin Wang, Guglielmo Scovazzi, Christopher E. Kees, Simone Rossi, Oriol Colomés, Alex Main. Dual-Scale Galerkin Methods for Darcy Flow., Journal of Computationa Physics, ( ): . doi:
TOTAL:	**1**	

Number of Papers published in peer-reviewed journals:

(b) Papers published in non-peer-reviewed journals (N/A for none)

Received		Paper
TOTAL:		

Number of Papers published in non peer-reviewed journals:

(c) Presentations

Number of Presentations: 2.00

Non Peer-Reviewed Conference Proceeding publications (other than abstracts):

Received Paper

TOTAL:

Number of Non Peer-Reviewed Conference Proceeding publications (other than abstracts):

Peer-Reviewed Conference Proceeding publications (other than abstracts):

Received Paper

TOTAL:

Number of Peer-Reviewed Conference Proceeding publications (other than abstracts):

(d) Manuscripts

Received Paper

TOTAL:

Number of Manuscripts:

Books

Received Book

TOTAL:

Received	Book Chapter

TOTAL:

Patents Submitted

Patents Awarded

Awards

G. Scovazzi: 2014 Early Career Award, Department of Energy (Advanced Scientific Computing Research).

G. Scovazzi: 2017 Presidential Early Career Award for Scientists and Engineers (PECASE).

Graduate Students

NAME	PERCENT_SUPPORTED
FTE Equivalent:	
Total Number:	

Names of Post Doctorates

NAME	PERCENT_SUPPORTED
FTE Equivalent:	
Total Number:	

Names of Faculty Supported

NAME	PERCENT_SUPPORTED
FTE Equivalent:	
Total Number:	

Names of Under Graduate students supported

NAME	PERCENT_SUPPORTED
FTE Equivalent:	
Total Number:	

Student Metrics

This section only applies to graduating undergraduates supported by this agreement in this reporting period

The number of undergraduates funded by this agreement who graduated during this period: 0.00

The number of undergraduates funded by this agreement who graduated during this period with a degree in science, mathematics, engineering, or technology fields:..... 0.00

The number of undergraduates funded by your agreement who graduated during this period and will continue to pursue a graduate or Ph.D. degree in science, mathematics, engineering, or technology fields:..... 0.00

Number of graduating undergraduates who achieved a 3.5 GPA to 4.0 (4.0 max scale):..... 0.00

Number of graduating undergraduates funded by a DoD funded Center of Excellence grant for Education, Research and Engineering:..... 0.00

The number of undergraduates funded by your agreement who graduated during this period and intend to work for the Department of Defense 0.00

The number of undergraduates funded by your agreement who graduated during this period and will receive scholarships or fellowships for further studies in science, mathematics, engineering or technology fields: 0.00

Names of Personnel receiving masters degrees

NAME

Total Number:

Names of personnel receiving PHDs

NAME

Total Number:

Names of other research staff

NAME	PERCENT_SUPPORTED

FTE Equivalent:

Total Number:

Sub Contractors (DD882)

Inventions (DD882)

Scientific Progress

See attachment.

Technology Transfer

The Dual-Scale DG method was implemented in PROTEUS, the computational framework developed by Chris Kees & Matthew Farthing at the Army Corps of Engineers, Computational Hydraulics Laboratory.
Broader impact can be also found in all army projects in which PROTEUS is used to solve porous media flows, such as simulation of levees, and variable density flows, saltwater intrusion in coastal aquifers.

Project Report: ARO Grant W911NF-13-1-0452
Dual-Scale Galerkin Methods for Darcy Flow

Guglielmo Scovazzi
Department of Civil and Environmental Engineering,
Duke University, Durham, North Carolina 27708

February 6, 2017

Abstract

The discontinuous Galerkin (DG) method has found widespread application in elliptic problems with rough coefficients, of which the Darcy flow equations are a prototypical example. One of the long-standing issues of DG approximations is the overall computational cost, and many different strategies have been proposed, such as the variational multiscale DG method, the hybridizable DG method, the multiscale DG method, the embedded DG method, and the Enriched Galerkin method. In this work, we propose a mixed dual-scale Galerkin method, in which the degrees-of-freedom of a less computationally expensive coarse-scale approximation are linked to the degrees-of-freedom of a base DG approximation. We show that the proposed approach has always similar or improved accuracy with respect to the base DG method, with a considerable reduction in computational cost. We provide a complete analysis of stability and convergence of the proposed method, in addition to a study on its conservation and consistency properties. In particular, we consider two cases for the definition of the coarse-scale space: 1) Raviart-Thomas finite elements for the mass flux and continuous linear finite elements for the pressure; 2) Continuous linear finite elements for both the flux and pressure. We also present a battery of numerical tests to verify the results of the analysis.

Keywords: Discontinuous Galerkin method; variational multiscale method; hybridization; elliptic problems; Darcy flow.

Contents

1 Forward

Discontinuous Galerkin (DG) methods are Galerkin variational methods in which the test and trial function spaces are discontinuous polynomials. They have been applied successfully to hyperbolic problems [35, 18, 14] and elliptic problems, with smooth [2, 1] and rough [19, 39, 20, 37, 21, 36] coefficients, in both primal and mixed form [30, 34, 6, 5, 13, 26, 28, 27, 29].

DG methods have reached popularity because of their advantages in the imposition of local conservation, the enforcement of general boundary conditions and the construction of data structures for parallel implementations.

However, the application of DG methods to large-scale engineering problems has often been hampered by the larger computational cost with respect to continuous Galerkin approximations, due to the relative increase of the number of degrees-of-freedom.

Several methods have been proposed to reduce the computational cost of DG methods: the variational multiscale approach, which yields a multiscale DG method with cost comparable to a continuous Galerkin method [24, 3, 11]; the hybridizable DG (HDG) method [15, 16, 32, 31], which utilizes hybridization approaches originally developed in the context of mixed finite element methods and, more recently, evolved in the embedded discontinuous Galerkin (EDG) method [17]; and,

finally, the enriched Galerkin (EG) method [25], which is based on a piecewise constant discontinuous enrichment of a base continuous Galerkin method.

The variational multiscale DG method [24, 3, 11] was developed based on the idea that the discontinuous solution can be decomposed as the sum of a continuous component and discontinuous correction. The discontinuous correction is then estimated using local condensation techniques.

The hybridizable discontinuous Galerkin methods were first developed to solve second-order elliptic problems [16]. In the HDG method, additional unknowns in the form of numerical traces are introduced at the element interfaces, and conservation is ensured by means of a global flux continuity equation. Hence all the finite elements are considered as separate subdomains and only the traces are computed directly in a global solve. The DG solution can then be post-processed solving local DG problems where the traces are enforcing the boundary conditions. HDG methods have been widely tested over different problems, however, for the lowest-order shape function, they do not reduce the computational cost. To obviate this problem, embedded discontinuous Galerkin (EDG) methods were introduced by means of a space of numerical traces that are globally continuous. However, EDG methods cannot ensure optimal convergence rates.

The enriched Galerkin (EG) method was developed by Sun and Liu [38], and is based on the idea of enriching with a piecewise constant discontinuous function a continuous Galerkin approximation, and to use the interior penalty(IP) DG framework to appropriately derive a consistent variational formulation. The piecewise-constant enrichment can be thought of as a stabilizing penalty term. The EG method has been applied to second-order elliptic equations [38], Stokes problems [4] and parabolic problems [25].

In this report, we propose a new dual-scale DG (DSDG) method in mixed form. We distinguish between the DG solution, or DG scale, and a coarse scale (CS) component of the solution. A transfer operator based on local elemental problems is built to link the degrees-of-freedom between the DG and CS components of the solution. Then, the DG solution is replaced by the transfer operator applied to the CS solution in every term in the base DG variational formulation, and a new method is constructed with a significant reduction of degrees-of-freedom with respect to the original DG method. This amount to solve the original DG formulation on the image of the transfer operator, which is a proper subspace of the DG solution space.

We present a full mathematical analysis of the method and we also show its local and global conservation properties. We conclude with a number of computational tests aiming at highlighting the robustness, stability and accuracy properties of the DSDG method.

2 Governing equations: Darcy flow

The canonical Darcy flow equations govern the transport of fluid in miscible fluid through a porous medium, and can be expressed as:

$$\boldsymbol{\Lambda}^{-1}\boldsymbol{\beta} + \nabla p = 0 \qquad \text{in } \Omega, \tag{1a}$$

$$\nabla \cdot \boldsymbol{\beta} = \phi \qquad \text{in } \Omega, \tag{1b}$$

$$p = p_D \qquad \text{on } \Gamma_D, \tag{1c}$$

$$\boldsymbol{\beta} \cdot \boldsymbol{n} = h_N \qquad \text{on } \Gamma_N, \tag{1d}$$

where $\boldsymbol{\Lambda}$ is the mobility tensor/permeability coefficient, $\Omega \subset \mathbb{R}^d$ is an open, bounded and convex polyhedral domain with $\partial\Omega$ denoting its boundary, Γ_D and Γ_N are subsets of $\partial\Omega$ on which we

impose Dirichlet and Neumann Boundary conditions, and $\phi \in L^2(\Omega)$ is the source or sink term of mass in the medium. Note that we have introduced the auxiliary variable $\boldsymbol{\beta}$, representing the mass flux across the porous medium. The Darcy flow equations are a homogenized macroscopic model of transport through porous media. The mathematical structure of the Darcy flow equations is a mixed form of the Laplace equation. In the following analysis, we assume $\boldsymbol{\Lambda}$ is a symmetric positive definite tensor.

3 General notation and definitions of discontinuous Galerkin methods

Let $\mathcal{T}_h = \bigcup K$ be the decomposition of the domain Ω into non-overlapping closed shape-regular elements K such that K covers Ω exactly and does not contains any hanging nodes [23, 12]. ∂K denotes the element boundary. Let h denote the mesh length scale (e.g., the largest element diameter), and $h^{\perp}$ a characteristic length in a direction approximately perpendicular to an edge or face of the mesh, respectively, in two or three dimensions (see also Fig.1). Namely:

$$h^{\perp} = \begin{cases} \frac{\mathrm{meas}(K_+)+\mathrm{meas}(K_-)}{2\,\mathrm{meas}(\partial K_+ \cap \partial K_-)}\,, & \text{if} \in \partial \mathrm{K} \backslash \partial\Omega\,, \\ \frac{\mathrm{meas}(K)}{\mathrm{meas}(\partial K \bigcap \partial\Omega)}\,, & \text{if} \in \partial \mathrm{K} \bigcap \partial\Omega\,, \end{cases}$$

where for an interior edge, K_+ and K_- are the elements on either side sharing the edge. In what follows, we consider regular grids, for which $h^{\perp}$ and h are related to each other, in the sense that there exist two constants $\xi_1, \xi_2 \in \mathbb{R}^+$, independent of the specific edge considered, such that:

$$\xi_1\, h \leq h^{\perp} \leq \xi_2\, h\,. \tag{2}$$

In what follows, especially in the context of proofs, we will consider h and $h^{\perp}$ interchangeable. The discontinuous Galerkin function spaces are defined as

$$S_d = \left\{ p \in L^2(\Omega) :\ p\,|_k \in \mathcal{P}^p(K)\ \forall K \in \mathcal{T}_h \right\},$$

$$\boldsymbol{V}_d = \left\{ \boldsymbol{\beta} \in \left(L^2(\Omega)\right)^d :\ \boldsymbol{\beta}\,|_k \in \left(\mathcal{P}^p(K)\right)^d\ \forall K \in \mathcal{T}_h \right\},$$

where $\mathcal{P}^p(k)$ is the space of polynomial functions of order at most p on K. For simplicity, we denote $\boldsymbol{M}_d = \boldsymbol{V}_d \times S_d$ and let the continuous Galerkin function spaces as the subspace of S_d and $\boldsymbol{V}_d$ consisted by continuous piecewise polynomials:

$$S_c = S_d \bigcap \mathbb{C}^0(\Omega)\,,$$

$$\boldsymbol{V}_c = \boldsymbol{V}_d \bigcap \left(\mathbb{C}^0(\Omega)\right)^d.$$

Similarly, we define $\boldsymbol{M}_c = \boldsymbol{V}_c \times S_c$. In addition we introduce the Raviart-Thomas space

$$\mathbb{RT}^0(K) = (\mathcal{P}^0(K))^d \oplus \boldsymbol{x}\mathcal{P}^0(K)\,.$$

We denote the $L^2(K)$ inner products over an element interior and its boundary as:

$$(v,w)_K = \int_K vw\,, \quad \langle v,w\rangle_{\partial K} = \int_{\partial K} vw\,.$$

Next, we introduce the average operator $\{\cdot\}$ and the jump operator $[\![\cdot]\!]$ for the discontinuous scalars and vector fields as follows [8, 9]:

$$\begin{aligned}
\{p\} &= \frac{1}{2}\left(p^+ + p^-\right), \\
\{\boldsymbol{\beta}\} &= \frac{1}{2}\left(\boldsymbol{\beta}^+ + \boldsymbol{\beta}^-\right), \\
[\![p]\!] &= p^+\boldsymbol{n}^+ + p^-\boldsymbol{n}^-, \\
[\![\boldsymbol{\beta}]\!] &= \boldsymbol{\beta}^+ \cdot \boldsymbol{n}^+ + \boldsymbol{\beta}^- \cdot \boldsymbol{n}^-,
\end{aligned}$$

where the plus and minus signs indicate the two sides of an element edge in 2D or face in 3D. Then it is relatively easy to prove the identity [7]:

$$\sum_K \langle w, \mathbf{v}\cdot\boldsymbol{n}\rangle_{\partial K} = \langle [\![w]\!], \{\mathbf{v}\}\rangle_{\mathcal{E}} + \langle \{w\}, [\![v]\!]\rangle_{\mathcal{E}_i}, \tag{3}$$

where $\mathcal{E}$ is the set of all edges of the mesh, and $\mathcal{E}_i = \mathcal{E} \setminus \Gamma$ is the set of all interior edges.

4 A base mixed discontinuous Galerkin method [9]

We start the discussion by considering the DG formulation in [8, 9] as a basis to construct, in Section 5, a variational dual-scale DG approximation. Multiplying the strong form of the Darcy flow equations (1a)–(1b) by the test function $(q, \boldsymbol{\tau}) \in \boldsymbol{M}_d$ and integrating over the element K of the finite element mesh, we obtain

$$\begin{aligned}
\int_K \boldsymbol{\Lambda}^{-1}\boldsymbol{\beta}\cdot\boldsymbol{\tau} + \int_K \nabla p\cdot\boldsymbol{\tau} &= \int_K \boldsymbol{\Lambda}^{-1}\boldsymbol{\beta}\cdot\boldsymbol{\tau} - \int_K p\nabla\cdot\boldsymbol{\tau} + \int_{\partial K} p\boldsymbol{\tau}\cdot\boldsymbol{n} = 0, \\
\int_K q\nabla\cdot\boldsymbol{\beta} &= -\int_K \boldsymbol{\beta}\cdot\nabla q + \int_{\partial K} q\boldsymbol{\beta}\cdot\boldsymbol{n} = \int_K q\phi\,.
\end{aligned}$$

Introducing the simplified notation, if we apply integration by parts to the second equation, and replace the boundary traces by the *numerical fluxes* $(\widehat{p}, \widehat{\boldsymbol{\beta}})$ we obtain

$$\left(\boldsymbol{\Lambda}^{-1}\boldsymbol{\beta}, \boldsymbol{\tau}\right)_K - \left(p, \nabla\cdot\boldsymbol{\tau}\right)_K + \langle \widehat{p}, \boldsymbol{\tau}\cdot\boldsymbol{n}\rangle_{\partial K} = 0, \tag{4}$$

$$\left(\boldsymbol{\nabla}\cdot\boldsymbol{\beta}, q\right)_K + \langle (\widehat{\boldsymbol{\beta}} - \boldsymbol{\beta})\cdot\boldsymbol{n}, q\rangle_{\partial K} = \left(\phi, q\right)_K. \tag{5}$$

The numerical fluxes accomplish the linking of the discontinuous polynomial approximations (and corresponding degrees-of-freedom) of the solution between neighboring elements. Summing over all the elements,

$$\begin{aligned}
\left(\boldsymbol{\Lambda}^{-1}\boldsymbol{\beta}, \boldsymbol{\tau}\right)_\Omega - \left(p, \nabla\cdot\boldsymbol{\tau}\right)_\Omega + \sum_K \langle \widehat{p}, \boldsymbol{\tau}\cdot\boldsymbol{n}\rangle_{\partial K} &= 0, \\
\left(\nabla\cdot\boldsymbol{\beta}, q\right)_\Omega + \sum_K \langle (\widehat{\boldsymbol{\beta}} - \boldsymbol{\beta})\cdot\boldsymbol{n}, q\rangle_{\partial K} &= \left(\phi, q\right)_\Omega.
\end{aligned}$$

By using the definition of jump and average operators and in turn, inserting the identity (3) into the previous equations yield:

$$
\begin{aligned}
\left(\boldsymbol{\Lambda}^{-1}\boldsymbol{\beta},\boldsymbol{\tau}\right)_{\Omega} - (p,\nabla\cdot\boldsymbol{\tau})_{\Omega} + \langle[\![\widehat{p}]\!],\{\boldsymbol{\tau}\}\rangle_{\mathcal{E}} + \langle\{\widehat{p}\}\,,[\![\boldsymbol{\tau}]\!]\rangle_{\mathcal{E}_i} &= 0\,,\\
(\nabla\cdot\boldsymbol{\beta},q)_{\Omega} + \langle[\![q]\!],\{\widehat{\boldsymbol{\beta}}-\boldsymbol{\beta}\}\rangle_{\mathcal{E}} + \langle\{q\}\,,[\![\widehat{\boldsymbol{\beta}}-\boldsymbol{\beta}]\!]\rangle_{\mathcal{E}_i} &= (\phi,q)_{\Omega}\,.
\end{aligned}
$$

Separating the terms involving boundary edges, we obtain

$$
\begin{aligned}
\left(\boldsymbol{\Lambda}^{-1}\boldsymbol{\beta},\boldsymbol{\tau}\right)_{\Omega} - (p,\nabla\cdot\boldsymbol{\tau})_{\Omega} + \langle\widehat{p},\boldsymbol{\tau}\cdot\boldsymbol{n}\rangle_{\Gamma_D} + \langle\widehat{p},\boldsymbol{\tau}\cdot\boldsymbol{n}\rangle_{\Gamma_N} + \langle 1,[\![\widehat{p}\boldsymbol{\tau}]\!]\rangle_{\mathcal{E}_i} &= 0\,,\\
(\nabla\cdot\boldsymbol{\beta},q)_{\Omega} + \langle q,(\widehat{\boldsymbol{\beta}}-\boldsymbol{\beta})\cdot\boldsymbol{n}\rangle_{\Gamma_D} + \langle q,(\widehat{\boldsymbol{\beta}}-\boldsymbol{\beta})\cdot\boldsymbol{n}\rangle_{\Gamma_N} + \langle 1,[\![q(\widehat{\boldsymbol{\beta}}-\boldsymbol{\beta})]\!]\rangle_{\mathcal{E}_i} &= (\phi,q)_{\Omega}\,.
\end{aligned}
$$

In the method proposed in [8, 9] (see also [1] for a general perspective), the following choice of numerical fluxes is made

$$
\begin{array}{lll}
\widehat{p}=\{p\}\,, & \widehat{\boldsymbol{\beta}}=\{\boldsymbol{\beta}\}+\alpha\,[\![p]\!], & \text{on } \mathcal{E}_i\,,\\
\widehat{p}=p_D, & \widehat{\boldsymbol{\beta}}=\boldsymbol{\beta}+\alpha\,(p-p_D)\boldsymbol{n}, & \text{on } \Gamma_D\,,\\
\widehat{p}=p, & \widehat{\boldsymbol{\beta}}\cdot\boldsymbol{n}=h_N, & \text{on } \Gamma_N\,,
\end{array}
$$

where the penalty coefficient α is defined as $\alpha=\tilde{\alpha}(h^{\perp})^{-1}\|\boldsymbol{\Lambda}\|$ with $\tilde{\alpha}>0$, and, consequently, the final formulation reads:

$$
\begin{aligned}
\left(\boldsymbol{\Lambda}^{-1}\boldsymbol{\beta},\boldsymbol{\tau}\right)_{\Omega} - (p,\nabla\cdot\boldsymbol{\tau})_{\Omega} + \langle\{p\}\,,[\![\boldsymbol{\tau}]\!]\rangle_{\mathcal{E}_i}&\\
+\langle p\boldsymbol{n},\boldsymbol{\tau}\rangle_{\Gamma_N} &= -\langle p_D\boldsymbol{n},\boldsymbol{\tau}\rangle_{\Gamma_D}\,, \qquad (6)\\
(\nabla\cdot\boldsymbol{\beta},q)_{\Omega} - \langle\{q\}\,,[\![\boldsymbol{\beta}]\!]\rangle_{\mathcal{E}_i} - \langle q,\boldsymbol{\beta}\cdot\mathbf{n}\rangle_{\Gamma_N}&\\
+\langle[\![q]\!],\alpha\,[\![p]\!]\rangle_{\mathcal{E}_i} + \langle q,\alpha\,p\rangle_{\Gamma_D} &= (\phi,q)_{\Omega} - \langle q,h_N\rangle_{\Gamma_N} + \langle q,\alpha\,p_D\rangle_{\Gamma_D}\,, \qquad (7)
\end{aligned}
$$

which, more simply, can be written as

$$
B(\boldsymbol{\beta},p;\boldsymbol{\tau},q) = L(\boldsymbol{\tau},q)\,, \qquad (8a)
$$

$$
\begin{aligned}
B(\boldsymbol{\beta},p;\boldsymbol{\tau},q) = {} & (\boldsymbol{\Lambda}^{-1}\boldsymbol{\beta},\boldsymbol{\tau})_{\Omega} - (p,\nabla\cdot\boldsymbol{\tau})_{\Omega} + \langle\{p\},[\![\boldsymbol{\tau}]\!]\rangle_{\mathcal{E}_i} + \langle p\boldsymbol{n},\boldsymbol{\tau}\rangle_{\Gamma_N}\\
& + (\nabla\cdot\boldsymbol{\beta},q) - \langle\{q\},[\![\boldsymbol{\beta}]\!]\rangle_{\mathcal{E}_i} - \langle q,\boldsymbol{\beta}\cdot n\rangle_{\Gamma_N} + \langle[\![q]\!],\alpha\,[\![p]\!]\rangle_{\mathcal{E}_i} + \langle q,\alpha\,p\rangle_{\Gamma_D}\,, \qquad (8b)
\end{aligned}
$$

$$
L(\boldsymbol{\tau},q) = -\langle p_D\boldsymbol{n},\boldsymbol{\tau}\rangle_{\Gamma_D} + (\phi,q) - \langle q,h_N\rangle_{\Gamma_N} + \langle q,\alpha\,p_D\rangle_{\Gamma_D}\,. \qquad (8c)
$$

5 Dual-scale discontinuous Galerkin (DSDG) formulation

The dual-scale DG method is an approach to reduce the computational cost of DG methods. The key idea is the introduction of a local problem, which is used to condense some of the DG degrees-of-freedom over each element as a function of global unknowns which are associated with continuous Galerkin discretizations.

5.1 Local mixed form

We return now to a variational formulation which is local to an element of the discretization. Consider again the element-wise problem, which, from now on, we denote as *local solver*:

$$
\begin{aligned}
\left(\boldsymbol{\Lambda}^{-1}\boldsymbol{\beta},\boldsymbol{\tau}\right)_{K} - (p,\nabla\cdot\boldsymbol{\tau})_{K} &= -\langle\widehat{p}\boldsymbol{n},\boldsymbol{\tau}\rangle_{\partial K}, \qquad (9a)\\
(\nabla\cdot\boldsymbol{\beta},q)_{K} - \langle\boldsymbol{\beta}\cdot\boldsymbol{n},q\rangle_{\partial K} &= -\langle\widehat{\boldsymbol{\beta}}\cdot\boldsymbol{n},q\rangle_{\partial K} + (\phi,q)_{K}\,. \qquad (9b)
\end{aligned}
$$

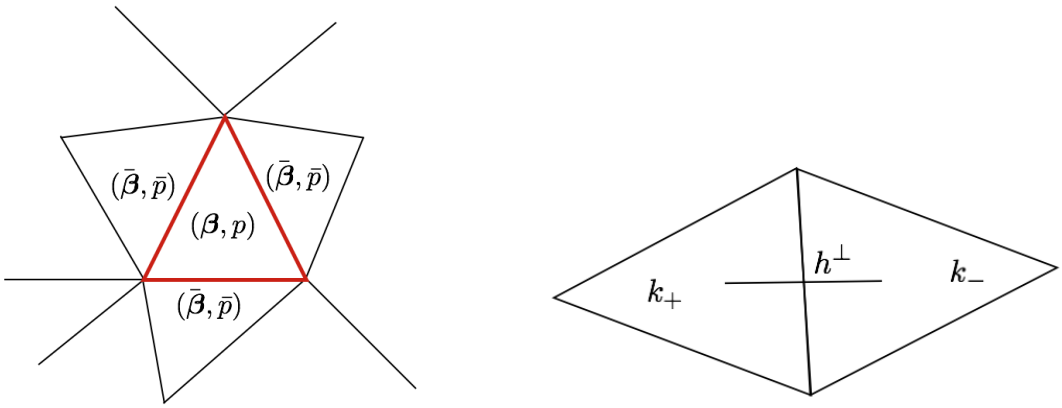

Figure 1: Left: Schematic representation of the local problem. Right: Illustration of $h^{\perp}$.

Here, for the sake of simplicity, we have considered the formulation in [9], but the same arguments can be generalized to the case of the method proposed in [1, 23, 7]. The local problem can be viewed as an element-wise DG problem in which the boundary conditions have been modified in order to create a link between the traces of the DG solution and the traces of a global discrete solution field that is less expensive to compute with, as shown in Fig. 1. To achieve this goal, the numerical fluxes are modified as follows:

$$\widehat{p} = \overline{p} + \alpha_p \left(\boldsymbol{\beta} - \overline{\boldsymbol{\beta}}\right) \cdot \boldsymbol{n}\,, \tag{10}$$

$$\widehat{\boldsymbol{\beta}} = \overline{\boldsymbol{\beta}} + \alpha_\beta \left(p - \overline{p}\right) \boldsymbol{n}\,. \tag{11}$$

where α_p and $\alpha_{\boldsymbol{\beta}}$ are penalties, defined as

$$\alpha_p = \tilde{\alpha}_p h^{\perp} \|\boldsymbol{\Lambda}\|^{-1}\,, \tag{12}$$

$$\alpha_{\boldsymbol{\beta}} = \tilde{\alpha}_{\boldsymbol{\beta}} (h^{\perp})^{-1} \|\boldsymbol{\Lambda}\|\,, \tag{13}$$

with $\tilde{\alpha}_p, \tilde{\alpha}_{\boldsymbol{\beta}} > 0$ and , $\|\boldsymbol{\Lambda}\|$ is the Frobenius norm of $\boldsymbol{\Lambda}$, coinciding with the eigenvalue $\lambda_{\max}$ of largest magnitude.

The terms $\overline{p}$ and $\overline{\boldsymbol{\beta}}$ are the traces of a discrete approximation associated with an interpolation different from the one of the base discontinuous Galerkin method. For example, we can introduce a space of globally continuous, piecewise-linear functions for the pressure p and a standard Raviart-Thomas space for the mass flux $\boldsymbol{\beta}$. In what follows, we will refer to this second set of interpolation spaces as the coarse-scale (CS) degrees-of-freedom. Note that the idea of imposing weak continuity between the boundary values of the pressure and mass flux of the DG and CS discrete fields is connected to the Steklov-Poincaré method in domain decomposition (see, e.g. [33]). We obtain:

$$\left(\boldsymbol{\Lambda}^{-1}\boldsymbol{\beta}, \boldsymbol{\tau}\right)_K - \left(p, \nabla \cdot \boldsymbol{\tau}\right)_K + \langle \alpha_p \boldsymbol{\beta} \cdot \boldsymbol{n}, \boldsymbol{\tau} \cdot \boldsymbol{n} \rangle_{\partial K} = -\langle \overline{p}, \boldsymbol{\tau} \cdot \boldsymbol{n} \rangle_{\partial K} + \langle \alpha_p \overline{\boldsymbol{\beta}} \cdot \boldsymbol{n}, \boldsymbol{\tau} \cdot \boldsymbol{n} \rangle_{\partial K}, \tag{14a}$$

$$\left(\nabla \cdot \boldsymbol{\beta}, q\right)_K - \langle \boldsymbol{\beta} \cdot \boldsymbol{n}, q \rangle_{\partial K} + \langle \alpha_\beta p \boldsymbol{n}, q \boldsymbol{n} \rangle_{\partial K} = -\langle \overline{\boldsymbol{\beta}} \cdot \boldsymbol{n}, q \rangle_{\partial K} + \langle \alpha_\beta \overline{p} \boldsymbol{n}, q \boldsymbol{n} \rangle_{\partial K} + \left(\phi, q\right)_K\,. \tag{14b}$$

The local problem is built with the idea that the CS fields can be used as boundary conditions in a weak formulation for the DG fields, with the purpose of designing a map between the CS and DG degrees-of-freedom. More specifically, the local problem defines a map/transfer operator $T_K : \boldsymbol{M}_c \to \boldsymbol{M}_d$. We can decompose the transfer operator into T^0, associated with the homogenous problem ($\phi = 0$), and a non-homogenous correction T_K^ϕ. Hence:

$$T_K(\cdot) = T_K^0(\cdot) + T_K^\phi \Phi$$

where Φ is the discrete array associated with the source term ϕ. In addition, we denote the global transfer operator T_Ω as the assembly of local transfer operators T_K's, that is $T_\Omega = \mathsf{A}_{K\in\mathcal{T}_h} T_K$, where A denotes the assembly operator.

On each element, we denote the image of transfer operator T_K by $R(T_K)$, a subset of the DG trial space. Correspondingly, $R(T_\Omega) \subset \boldsymbol{M}_d$ is the image of the global transfer operator T_Ω. Similarly, we can define the homogeneous global transfer operator T_Ω^0 and its image $R(T_\Omega^0)$.

In order to derive an algebraic problem linking the degrees-of-freedom of the DG and CS approximations, we introduce the local bilinear forms

$$\begin{aligned}
\widetilde{a}_K(\boldsymbol{\beta},\boldsymbol{\tau}) &= \left(\boldsymbol{\Lambda^{-1}}\boldsymbol{\beta},\boldsymbol{\tau}\right)_K + \langle \alpha_p \boldsymbol{\beta}\cdot\boldsymbol{n}, \boldsymbol{\tau}\cdot\boldsymbol{n}\rangle_{\partial K},\\
\widetilde{b}_K(p,\boldsymbol{\tau}) &= -\left(p, \nabla\boldsymbol{\tau}\right)_K,\\
\widetilde{c}_K(\boldsymbol{\beta},q) &= \left(\nabla\cdot\boldsymbol{\beta}, q\right)_K - \langle \boldsymbol{\beta}\cdot\boldsymbol{n}, q\rangle_{\partial K},\\
\widetilde{d}_K(p,q) &= \langle \alpha_\beta p\boldsymbol{n}, q\boldsymbol{n}\rangle_{\partial K},
\end{aligned}$$

and

$$\begin{aligned}
\overline{a}_K(\boldsymbol{\beta},\boldsymbol{\tau}) &= \langle \alpha_p \overline{\boldsymbol{\beta}}\cdot\boldsymbol{n}, \boldsymbol{\tau}\cdot\boldsymbol{n}\rangle_{\partial K},\\
\overline{b}_K(p,\boldsymbol{\tau}) &= -\langle \overline{p}, \boldsymbol{\tau}\cdot\boldsymbol{n}\rangle_{\partial K},\\
\overline{c}_K(\boldsymbol{\beta},q) &= -\langle \overline{\boldsymbol{\beta}}\cdot\boldsymbol{n}, q\rangle_{\partial K},\\
\overline{d}_K(p,q) &= \langle \alpha_\beta \overline{p}\boldsymbol{n}, q\boldsymbol{n}\rangle_{\partial K},
\end{aligned}$$

and the linear form

$$\mathbf{F}_K(q) = \left(\phi, q\right)_K.$$

Using the shape functions associated with the DG and CS spaces, we can finally obtain algebraic equations linking the local degrees-of-freedom of the two discretizations. To this end, we introduce the matrices

$$\widetilde{\mathbb{M}}_K = \begin{bmatrix} \widetilde{\mathbb{A}}_K & \widetilde{\mathbb{B}}_K \\ \widetilde{\mathbb{C}}_K & \widetilde{\mathbb{D}}_K \end{bmatrix}, \qquad \overline{\mathbb{M}}_K = \begin{bmatrix} \overline{\mathbb{A}}_K & \overline{\mathbb{B}}_K \\ \overline{\mathbb{C}}_K & \overline{\mathbb{D}}_K \end{bmatrix},$$

where $[\widetilde{\mathbb{A}}_K]_{ab;ij} = \widetilde{a}_K(N_a\boldsymbol{e_i}, N_b\boldsymbol{e_j})$, $[\widetilde{\mathbb{B}}_K]_{ab;i} = \widetilde{b}_K(N_a\boldsymbol{e_i}, N_b)$, etc. These matrices are instrumental in developing an algebraic transfer operator between the CS and DG solution. Denoting by $\mathbf{Y}_K$ the vector of degrees-of-freedom associated with the solution $(p,\boldsymbol{\beta})$ over the element K, we obtain:

$$\boldsymbol{Y}_K = \mathbb{T}_K^0 \bar{\boldsymbol{Y}}_K + \mathbb{T}_K^\phi \mathbf{F}_K\,, \tag{15a}$$

where

$$\mathbb{T}_K^0 = \widetilde{\mathbb{M}}_K^{-1}\overline{\mathbb{M}}_K\,, \tag{15b}$$

$$\mathbb{T}_K^\phi = \widetilde{\mathbb{M}}_K^{-1}\,, \tag{15c}$$

are the algebraic version of the transfer maps between the CS and DG degrees-of-freedom. The algebraic transfer operators, since the stiffness matrix $\widetilde{\mathbb{M}}_K$ associated with the well-posed base DG formulation, is invertible by construction. The transfer map can be used in computations by means of a static condensation procedure.

5.2 DSDG global formulation

Starting from the general mixed form [9] of the DG problem, which amounts to seeking $(\boldsymbol{\beta}, p) \in \boldsymbol{M}_d$ such that

$$B(\boldsymbol{\beta}, p; \boldsymbol{\tau}, q) = L(\boldsymbol{\tau}, q)\,, \quad \forall\,(\boldsymbol{\tau}, q) \in \boldsymbol{M}_d \tag{16}$$

we use the global transfer operator T_Ω to express

$$\begin{aligned}(\boldsymbol{\beta}, p) &= T_\Omega\left(\boldsymbol{\beta}_c, p_c\right)\,,\\ (\boldsymbol{\tau}, q) &= T_\Omega^0\left(\boldsymbol{\tau}_c, q_c\right)\,.\end{aligned}$$

The previous equations need to be understood as follows: $(\boldsymbol{\beta}, p) = T_\Omega\left(\boldsymbol{\beta}_c, p_c\right)$ indicates that the fields $(\boldsymbol{\beta}, p)$ can be generated by degrees-of-freedoms that are mapped through the transfer operator T_Ω from the degrees-of-freedom associated with $(\boldsymbol{\beta}_c, p_c)$. Then we can generate the DSDG problem, in which we seek $(\boldsymbol{\beta}_c, p_c) \in \boldsymbol{M}_c$, such that

$$B\left(T_\Omega\left(\boldsymbol{\beta}_c, p_c\right); T_\Omega^0\left(\boldsymbol{\tau}_c, q_c\right)\right) = L\left(T_\Omega^0\left(\boldsymbol{\tau}_c, q_c\right)\right)\,, \quad \forall\,(\boldsymbol{\tau}_c, q_c) \in \boldsymbol{M}_c\,. \tag{17}$$

This formulation represents the key strategy in simplifying the DG problem to a simpler problem of finding the solution in terms of the CS degrees-of-freedom. Equivalent variational statement are:

Seek $(\boldsymbol{\beta}, p) \in R\left(T_\Omega\right)$, such that

$$B\left(\boldsymbol{\beta}, p; \boldsymbol{\tau}, q\right) = L\left(\boldsymbol{\tau}, q\right)\,, \quad \forall\,(\boldsymbol{\tau}, q) \in R\left(T_\Omega^0\right)\,, \tag{18}$$

Seek $(\boldsymbol{\beta}, p) \in R\left(T_\Omega^0\right)$, such that

$$B\left(\boldsymbol{\beta}, p; \boldsymbol{\tau}, q\right) = L^0\left(\boldsymbol{\tau}, q\right)\,, \quad \forall\,(\boldsymbol{\tau}, q) \in R\left(T_\Omega^0\right)\,, \tag{19}$$

where $L^0\left(\boldsymbol{\tau}, q\right) = L\left(\boldsymbol{\tau}, q\right) - B\left(T_\Omega^\phi \Phi; \boldsymbol{\tau}, q\right)$.

5.3 Assembly

Whenever the DG degrees-of-freedom appear in the local assembly matrices, they can be replaced through the transfer map using the CS degrees of freedom. Analogously, we use the transfer operator to transfer the DG test space to the space, by applying $\mathbb{T}_K^0$ to the vector of test function degrees-of-freedom W, that is,

$$W_K = \mathbb{T}^0_K \bar{W}_K.$$

In the final assembly of the local matrices, the connectivity data structure of the CS method is used in place of the DG one, with a substantial reduction in the number of degrees-of-freedom. Note also that once a CS solution is computed, the DG solution can be post-processed using once again the CS-to-DG transfer map. This strategy has similarities with the variational multiscale DG method proposed by one of the authors in [24] and hybridizable DG methods, proposed a few years later in [15].

Because in DG methods the shape functions relative to an element are supported (i.e., non-zero) only on that element, it is possible to give a global algebraic interpretation to the strategy pursued, once the full assembly of the system is considered. If $\boldsymbol{A}_K$ is the elemental (local) matrix associated with the DG method described in Section 4, the global system can be assembled as:

$$\text{Assemble}\left[\bar{W}_K^T \left(\mathbb{T}^0_K\right)^T \boldsymbol{A}_K \left(\mathbb{T}^0_K \bar{\boldsymbol{Y}}_K + \mathbb{T}^\phi_K F_K\right)\right] = \text{Assemble}\left[\bar{W}_K^T \left(\mathbb{T}^0_K\right)^T \mathbf{F}_K\right] \tag{20}$$

and, once the assembly is performed,

$$\bar{W}^T \left(\mathbb{T}^0_\Omega\right)^T \boldsymbol{A}\, \mathbb{T}^0_\Omega \bar{\boldsymbol{Y}} = \bar{W}^T \left(\mathbb{T}^0_\Omega\right)^T \left(\boldsymbol{I} - \boldsymbol{A}\, \mathbb{T}^\phi_\Omega\right) \mathbf{F}\,, \tag{21}$$

where $\boldsymbol{A}$ is the global matrix associated to the original DG formulation, T^Y is the global transfer operator from the CS to the DG degrees-of-freedom, and we indicate by B^T the transpose of a matrix B. Observe that the new algebraic system considered has a reduced global number of degrees-of-freedom with respect to the original DG algebraic system. Also observe that while the global algebraic equation (21) provides a general interpretation of the proposed method, it is never implemented as is, but instead (20) is used in computations.

6 Multigrid interpretation of the DSDG method

The DG formulation (16) leads to the algebraic system

$$\boldsymbol{A}\,\boldsymbol{Y} = \boldsymbol{F}$$

where $\boldsymbol{A}$ is the stiffness (Jacobian) matrix, $\boldsymbol{Y}$ is the DG degree-of-freedom vector and $\boldsymbol{F}$ is the right-hand-side vector. The corresponding DSDG formulation (19) leads to

$$\boldsymbol{T}^T \boldsymbol{A}\, \boldsymbol{T}\, \boldsymbol{Y}^{CS} = \boldsymbol{T}^T \boldsymbol{F} - \boldsymbol{T}^T \boldsymbol{\Phi}$$

where $\boldsymbol{T}$ is the assembly of local transfer operator matrix of size (DG global DoFs)$\times$(CS global DoFs), $\boldsymbol{Y}^{CS}$ is the CS degree-of-freedom vector and $\boldsymbol{\Phi}$ is the vector of transferred right hand side term calculated from the term $B\left(T^\phi_\Omega \Phi; T^0_\Omega(\boldsymbol{\tau}, q)\right)$ in (19). Defining $\boldsymbol{F}^0 = \boldsymbol{F} - \boldsymbol{\Phi}$ and $\boldsymbol{A}^{CS} = \boldsymbol{T}^T \boldsymbol{A}\, \boldsymbol{T}$, we can equivalently write

$$\boldsymbol{A}^{CS}\, \boldsymbol{Y}^{CS} = \boldsymbol{T}^T \boldsymbol{F}^0\,.$$

Introducing the algebraic residual

$$\boldsymbol{r} = \boldsymbol{F} - \boldsymbol{A}\,\boldsymbol{Y}$$

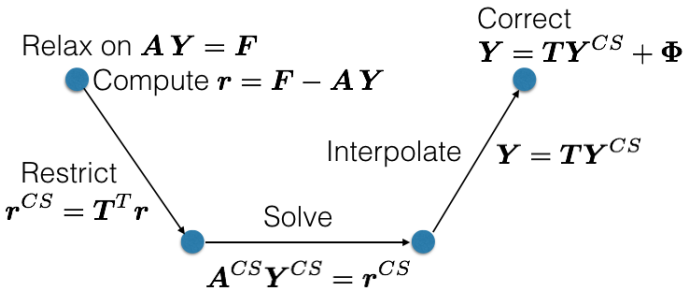

Figure 2: Multigrid illustration

we can correspondingly write

$$\boldsymbol{r}^{CS} = \boldsymbol{T}^T\boldsymbol{r} = \boldsymbol{T}^T\left(\boldsymbol{F}^0 - \boldsymbol{A}\boldsymbol{T}\boldsymbol{Y}^{CS}\right) .$$

Then the DSDG approach can also be described as a one-level V-cycle multigrid scheme [10] as shown in Figure 2, where $\boldsymbol{Y}$ is interpreted as fine scale solution, $\boldsymbol{Y}^{CS}$ is interpreted as the coarse scale solution, $\boldsymbol{T}$ is treated as the restriction matrix and $\boldsymbol{T}^T$ is treated as the interpolation matrix. Namely:

1. Relax $\boldsymbol{A}\boldsymbol{Y} = \boldsymbol{F}$, with initial guess $\boldsymbol{0}$.
2. Compute $\boldsymbol{r} = \boldsymbol{F} - \boldsymbol{A}\boldsymbol{Y} = \boldsymbol{F}$.
3. Compute $\boldsymbol{r}^{CS} = \boldsymbol{T}^T\boldsymbol{r}$.
4. Solve the coarse solution $\boldsymbol{A}^{CS}\boldsymbol{Y}^{CS} = \boldsymbol{r}^{CS}$.
5. Correct the fine grid solution $\boldsymbol{Y} = \boldsymbol{T}\boldsymbol{Y}^{CS} + \boldsymbol{\Phi}$.

Notice that unlike in regular multigrid methods, the DSDG method uses the same map for the fine and coarse grids but with different degree-of-freedoms.

7 Preliminaries: Analysis of the base DG formulation [9]

We begin by recalling a number of fundamental results on the well-posedness of the base DG formulation [9].

Proposition 1 (Consistency/Galerkin orthogonality)**.** *Let* $(\boldsymbol{\beta}_e, p_e)$ *be the exact solution to* (1) *and* $(\boldsymbol{\beta}, p) \in \boldsymbol{M}_d$ *the discrete solution to* (8)*, then* $\forall\,(\boldsymbol{\tau}, q) \in \boldsymbol{M}_d$*,* $B(\boldsymbol{\beta}_e - \boldsymbol{\beta}, p_e - p; \tau, q) = 0$.

Proof. Substituting the exact solution ($\boldsymbol{\beta}_e$, p_e) into the global DG formulation, we get:

$$\begin{aligned} B(\boldsymbol{\beta}_e, p_e; \tau, q) = {} & (\boldsymbol{\Lambda}^{-1}\boldsymbol{\beta}_e, \boldsymbol{\tau})_\Omega - (p_e, \nabla\cdot\boldsymbol{\tau})_\Omega + \langle\{p_e\}, [\![\boldsymbol{\tau}]\!]\rangle_{\mathcal{E}_i} + \langle p_e\boldsymbol{n}, \boldsymbol{\tau}\rangle_{\Gamma_N} \\ & + (\nabla\cdot\boldsymbol{\beta}_e, q)_\Omega - \langle[\![\boldsymbol{\beta}_e]\!], \{q\}\rangle_{\mathcal{E}_i} - \langle\boldsymbol{\beta}\cdot\boldsymbol{n}, q\rangle_{\Gamma_N} + \langle\alpha[\![p_e]\!], [\![q]\!]\rangle_{\mathcal{E}_i} + \langle\alpha p_e, q\rangle_{\Gamma_D} . \end{aligned} \tag{22}$$

Integrating by parts and using the identity (3) yield:

$$B(\boldsymbol{\beta}_e, p_e; \tau, q) = (\boldsymbol{\Lambda}^{-1}\boldsymbol{\beta}_e, \boldsymbol{\tau})_\Omega + (\nabla p_e, \boldsymbol{\tau})_\Omega - \langle p_e \boldsymbol{n}, \boldsymbol{\tau}\rangle_{\Gamma_D} + (\nabla \cdot \boldsymbol{\beta}_e, q)_\Omega - \langle [\![\boldsymbol{\beta}_e]\!], \{q\}\rangle_{\mathcal{E}_i} - \langle \boldsymbol{\beta}\cdot\boldsymbol{n}, q\rangle_{\Gamma_N} + \langle \alpha [\![p_e]\!], [\![q]\!]\rangle + \langle \alpha p_e, q\rangle_{\Gamma_D} . \quad (23)$$

Since the exact solution satisfies $[\![p_e]\!] = 0$ and $[\![\boldsymbol{\beta}_e]\!] = 0$, the bilinear form simplifies to

$$B(\boldsymbol{\beta}_e, p_e; \boldsymbol{\tau}, q) - L(\boldsymbol{\tau}, q) = (\boldsymbol{\Lambda}^{-1}\boldsymbol{\beta}_e + \nabla p_e, \boldsymbol{\tau})_\Omega + (\nabla\cdot\boldsymbol{\beta}_e - \phi, q)_\Omega + \langle (p_D - p_e)\boldsymbol{n}, \boldsymbol{\tau}\rangle_{\Gamma_D} - \langle (h_N - \boldsymbol{\beta}\cdot\boldsymbol{n}), q\rangle_{\Gamma_N} + \langle \alpha(p_D - p_e), q\rangle_{\Gamma_D} = 0 . \quad (24)$$

Then $\boldsymbol{\beta}_e$, p_e satisfies the DG formulation (8), and, consequently

$$B(\boldsymbol{\beta}_e - \boldsymbol{\beta}, p_e - p; \tau, p) = 0 , \quad (25)$$

implying that the global DG formulation (8) is consistent. □

Proposition 2 (Uniqueness)**.** *For $\tilde{\alpha} > 0$, then, if the solution to* (8) *exists, it is unique.*

Proof. Due to linearity, proving uniqueness is equivalent to show that the only solution of the homogenous problem ($p_D = 0$, $h_N = 0$, $\phi = 0$) associated with (8) is the zero solution ($\boldsymbol{\beta} = \mathbf{0}$ and $p = 0$). Summing (6)–(7), with the substitutions $\boldsymbol{\tau} = \boldsymbol{\beta}$ and $q = p$, yields

$$(\boldsymbol{\Lambda}^{-1}\boldsymbol{\beta}, \boldsymbol{\beta})_\Omega + \langle [\![p]\!], \alpha\, [\![p]\!]\rangle_{\mathcal{E}_i} + \langle p, \alpha\, p\rangle_{\Gamma_D} = 0 . \quad (26)$$

Since $\alpha > 0$ and $\boldsymbol{\Lambda}$ is positive definite, then all the three terms in the previous equation are non-negative. Then the only possibility is that all three terms vanish, which implies that $\boldsymbol{\beta} = 0$ on the interior of the domain, $[\![p]\!] = 0$ on the interior edges, and $p = 0$ on the Dirichlet boundary. Substituting these back into (6), we have

$$-(p, \nabla\cdot\boldsymbol{\tau})_\Omega + \langle \{p\}, [\![\boldsymbol{\tau}]\!]\rangle_{\mathcal{E}_i} + \langle pn, \boldsymbol{\tau}\rangle_{\Gamma_N} = 0 . \quad (27)$$

Integrating by parts and using (3) we obtain

$$(\nabla p, \boldsymbol{\tau})_\Omega - \langle [\![p]\!], \{\boldsymbol{\tau}\}\rangle_{\mathcal{E}_i} - \langle pn, \boldsymbol{\tau}\rangle_{\Gamma_D} = (\nabla p, \boldsymbol{\tau})_\Omega = 0 , \qquad \forall \boldsymbol{\tau} . \quad (28)$$

Hence, $\nabla p = 0$ over the interior of the domain, which means that p is constant. Because of the homogenous Dirichlet condition $p = 0$ and the jump condition $[\![p]\!] = 0$ implies that $p = 0$ over the entire domain. Hence $p = 0$ and $\boldsymbol{\beta} = 0$ for homogeneous conditions. □

Proposition 3 (Coercivity)**.** *There exists a constant c_L, such that, $\forall\, (\boldsymbol{\beta}, p) \in \boldsymbol{M}_d$,*

$$c_L B\left(\boldsymbol{\beta}, p; \boldsymbol{\beta}, p\right) \geq \|\boldsymbol{\Lambda}^{-1/2}\boldsymbol{\beta}\|_\Omega + \|(h^\perp)^{-1/2}\|\boldsymbol{\Lambda}\|^{1/2}[\![p]\!]\|_{\mathcal{E}\setminus\Gamma_N} .$$

Proof. Following the steps in the proof of Theorem 2, the DG bilinear form can be simplified to

$$\begin{aligned} B\left(\boldsymbol{\beta}, p; \boldsymbol{\beta}, p\right) &= \left(\boldsymbol{\Lambda}^{-1}\boldsymbol{\beta}, \boldsymbol{\beta}\right)_\Omega + \langle \alpha [\![p]\!], [\![p]\!]\rangle_{\varepsilon\setminus\Gamma_N} \\ &= \left(\boldsymbol{\Lambda}^{-1}\boldsymbol{\beta}, \boldsymbol{\beta}\right)_\Omega + \tilde{\alpha}\langle \|\boldsymbol{\Lambda}\|/h^\perp [\![p]\!], [\![p]\!]\rangle_{\mathcal{E}\setminus\Gamma_N} \\ &= \|\boldsymbol{\Lambda}^{-1/2}\boldsymbol{\beta}\|_\Omega + \tilde{\alpha}\|(h^\perp)^{-1/2}\|\boldsymbol{\Lambda}\|^{1/2}[\![p]\!]\|_{\mathcal{E}\setminus\Gamma_N} . \end{aligned}$$

We conclude by taking $c_L = 1/\max(1, \tilde{\alpha})$. □

The existence of the solution can be proved by establishing an inf-sup/LBB-type condition, as shown in [9]. The proof is actually almost identical to the proof of Theorem 1, which we state later in the context of the DSDG method.

Proposition 4 (Conservation)**.** *The base DG formulation is both locally and globally conservative.*

Proof. Applying the test function $(\boldsymbol{\tau} = 0, q = 1) \in \boldsymbol{M}_d(K)$ to the elemental variational DG formulation (4)–(5) yields

$$(\boldsymbol{\nabla} \cdot \boldsymbol{\beta}, 1)_K + \langle (\widehat{\boldsymbol{\beta}} - \boldsymbol{\beta}) \cdot \boldsymbol{n}, 1 \rangle_{\partial K} = (\phi, q)_K \ .$$

Integration by parts yields

$$\langle \boldsymbol{\beta} \cdot \boldsymbol{n}, 1 \rangle_{\partial K} - (\boldsymbol{\beta}, \nabla 1)_K + \langle (\widehat{\boldsymbol{\beta}} - \boldsymbol{\beta}) \cdot \boldsymbol{n}, 1 \rangle_{\partial K} = (\phi, 1)_K \ ,$$

that is

$$\langle \widehat{\boldsymbol{\beta}} \cdot \boldsymbol{n}, 1 \rangle_{\partial K} = (\phi, 1)_K \ . \tag{29}$$

Hence, the base DG method is locally conservative with respect to the numerical flux $\hat{\boldsymbol{\beta}}$. Summing (29) over all elements yields

$$\langle \widehat{\boldsymbol{\beta}} \cdot \boldsymbol{n}, 1 \rangle_{\partial K \bigcap \partial \Omega} = (\phi, 1)_\Omega \ ,$$

which is a global statement of conservation. □

8 Analysis of the dual-scale DG method

The general idea and theme in the analysis of the DSDG method is to first discuss the properties of the transfer operators and show they are injective and have fixed points. Then, in a second stage, these local properties are used to prove statements of consistency, conservation, and well-posedness of the overall DSDG formulation. In particular, the well-posedness of the global formulation will be proved introducing and proving a LBB/inf-sup condition on the range of the transfer operator.

Proposition 5. *Let $\lambda_{\max}$ be the largest eigenvalue of the symmetric positive definite permeability tensor $\boldsymbol{\Lambda}$. Assume $\tilde{\alpha}_p > \lambda_{\max}/2$ and $\tilde{\alpha}_{\boldsymbol{\beta}} > 1/(2\,\lambda_{max})$, then there exist a unique solution $(\boldsymbol{\beta}, p)$ to the local problem* (14a)–(14b)*.*

Proof. We adapt here a proof from [8]. Because we are in the case of finite-dimensional discrete spaces, the existence and uniqueness for the solution of the local problem is equivalent to showing that $\boldsymbol{\beta} = 0$ and $p = 0$ is the only solution of the homogenous problem (i.e., with $\bar{\boldsymbol{\beta}} = 0$, $\bar{p} = 0$. Setting $\bar{\boldsymbol{\beta}} = 0$, $\bar{p} = 0$ and $\phi = 0$ in (14a)–(14b), we obtain:

$$(\boldsymbol{\Lambda}^{-1}\boldsymbol{\beta}, \boldsymbol{\tau})_K - (p, \nabla \cdot \boldsymbol{\tau})_K + \langle \alpha_p \boldsymbol{\beta} \cdot \boldsymbol{n}, \boldsymbol{\tau} \cdot \boldsymbol{n} \rangle_{\partial K} = 0 \,, \tag{30}$$

$$(\nabla \cdot \boldsymbol{\beta}, q)_K - \langle \boldsymbol{\beta} \cdot n, q \rangle_{\partial K} + \langle \alpha_{\boldsymbol{\beta}} p, q \rangle_{\partial K} = 0 \,, \tag{31}$$

which hold for any $\boldsymbol{\tau}$ and q. Taking $\boldsymbol{\tau} = \boldsymbol{\beta}$ and $q = p$, we have

$$(\boldsymbol{\Lambda}^{-1}\boldsymbol{\beta}, \boldsymbol{\beta})_K - (p, \nabla \cdot \boldsymbol{\beta})_K + \langle \alpha_p \boldsymbol{\beta} \cdot \boldsymbol{n}, \boldsymbol{\beta} \cdot \boldsymbol{n} \rangle_{\partial K} = 0 \,, \tag{32}$$

$$(\nabla \cdot \boldsymbol{\beta}, p)_K - \langle \boldsymbol{\beta} \cdot \boldsymbol{n}, p \rangle_{\partial K} + \langle \alpha_{\boldsymbol{\beta}} p, p \rangle_{\partial K} = 0 \,, \tag{33}$$

which, when summed, result in

$$(\boldsymbol{\Lambda}^{-1}\boldsymbol{\beta},\boldsymbol{\beta})_K - \langle \boldsymbol{\beta}\cdot\boldsymbol{n}, p\rangle_{\partial K} + \langle \alpha_p \boldsymbol{\beta}\cdot\boldsymbol{n}, \boldsymbol{\beta}\cdot\boldsymbol{n}\rangle_{\partial K} + \langle \alpha_{\boldsymbol{\beta}} p, p\rangle_{\partial K} = 0\,. \tag{34}$$

Substituting the definition of penalty terms (12)–(13) into (34), we also get

$$(\boldsymbol{\Lambda}^{-1}\boldsymbol{\beta},\boldsymbol{\beta})_K - \langle \boldsymbol{\beta}\cdot\boldsymbol{n}, p\rangle_{\partial K} + \langle \tilde{\alpha}_p h^\perp \|\boldsymbol{\Lambda}\|^{-1}\boldsymbol{\beta}\cdot\boldsymbol{n}, \boldsymbol{\beta}\cdot\boldsymbol{n}\rangle_{\partial K} + \langle \tilde{\alpha}_{\boldsymbol{\beta}} (h^\perp)^{-1}\|\boldsymbol{\Lambda}\| p, p\rangle_{\partial K} = 0\,. \tag{35}$$

We now introduce the identity

$$\begin{aligned}
\langle \boldsymbol{\beta}\cdot\boldsymbol{n}, p\rangle_{\partial K} &= \langle (h^\perp)^{1/2}\boldsymbol{\beta}\cdot\boldsymbol{n}, (h^\perp)^{-1/2} p\rangle_{\partial K} \\
&= \frac{1}{2}\left(\langle (h^\perp)\boldsymbol{\beta}\cdot\boldsymbol{n}, \boldsymbol{\beta}\cdot\boldsymbol{n}\rangle_{\partial K} + \langle (h^\perp)^{-1} p, p\rangle_{\partial K}\right) \\
&\quad - \frac{1}{2}\langle (h^\perp)^{1/2}\boldsymbol{\beta}\cdot\boldsymbol{n} - (h^\perp)^{-1/2} p, (h^\perp)^{1/2}\boldsymbol{\beta}\cdot\boldsymbol{n} - (h^\perp)^{-1/2} p\rangle_{\partial K}\,,
\end{aligned} \tag{36}$$

which, substituted into (35), yields

$$\begin{aligned}
&(\boldsymbol{\Lambda}^{-1}\boldsymbol{\beta},\boldsymbol{\beta})_K + \frac{1}{2}\langle (h^\perp)^{1/2}\boldsymbol{\beta}\cdot\boldsymbol{n} - (h^\perp)^{-1/2} p, (h^\perp)^{1/2}\boldsymbol{\beta}\cdot\boldsymbol{n} - (h^\perp)^{-1/2} p\rangle_{\partial K} \\
&\quad + \langle (h^\perp)(\tilde{\alpha}_p\|\boldsymbol{\Lambda}\|^{-1} - 1/2)\boldsymbol{\beta}\cdot\boldsymbol{n}, \boldsymbol{\beta}\cdot\boldsymbol{n}\rangle_{\partial K} + \langle (h^\perp)^{-1}(\tilde{\alpha}_{\boldsymbol{\beta}}\|\boldsymbol{\Lambda}\| - 1/2) p, p\rangle_{\partial K} = 0\,.
\end{aligned} \tag{37}$$

The first two terms are non-negative, and to guarantee the third and fourth terms are non-negative, we need to require $\tilde{\alpha}_p \geq \|\boldsymbol{\Lambda}\|/2 = \lambda_{\max}/2$ and $\tilde{\alpha}_{\boldsymbol{\beta}} > 1/(2\|\boldsymbol{\Lambda}\|) = 1/(2\lambda_{\max})$, respectively. Under these conditions all the terms in (37) are non-negative, and they have to add up to zero, implying that $\boldsymbol{\beta} = \boldsymbol{0}$ in the interior of K, and $\boldsymbol{\beta}\cdot\boldsymbol{n} = 0$ and $p = 0$ on the boundary. Substituting these results back into (30), we derive that $(p, \nabla\cdot\boldsymbol{\tau})_K = 0$, which, combined with the fact that $p = 0$ on the boundary implies that $p = 0$ everywhere on K. □

Corollary 1. *Assume the conditions of Proposition 5 hold, and that $\alpha_p\alpha_{\boldsymbol{\beta}} \neq 1$. Then the local transfer operator associated with (14a)–(14b) is injective.*

Proof. Recalling the definition of the transfer operator from $\bar{\boldsymbol{Y}}_K$ to $\boldsymbol{Y}_K$, we can define $\boldsymbol{Y}_{1;K} = \mathbb{T}_K^0\bar{\boldsymbol{Y}}_{1;K} + \mathbb{T}_K^\phi\mathbf{F}_K$ and $\boldsymbol{Y}_{2;K} = \mathbb{T}_K^0\bar{\boldsymbol{Y}}_{2;K} + \mathbb{T}_K^\phi\mathbf{F}_K$ and observe that $\boldsymbol{Y}_{1;K} = \boldsymbol{Y}_{2;K}$ implies that $\mathbb{T}_K^0\bar{\boldsymbol{Y}}_{1;K} = \mathbb{T}_K^0\bar{\boldsymbol{Y}}_{2;K}$, that is $\tilde{\mathbb{M}}^{-1}\bar{\mathbb{M}}\,\bar{\boldsymbol{Y}}_{1;K} = \tilde{\mathbb{M}}^{-1}\bar{\mathbb{M}}\,\bar{\boldsymbol{Y}}_{2;K}$. Now, $\tilde{\mathbb{M}}$ is bijective by Proposition 5, so that the previous equality collapses to $\bar{\mathbb{M}}\,\bar{\boldsymbol{Y}}_{1;K} = \bar{\mathbb{M}}\,\bar{\boldsymbol{Y}}_{2;K}$. Then the injectivity of the transfer operator boils down to the injectivity of $\bar{\mathbb{M}}$, which can be equivalently stated by saying that

$$\begin{aligned}
-\langle \bar{p}_1, \boldsymbol{\tau}\cdot\boldsymbol{n}\rangle_{\partial K} + \langle \alpha_p\bar{\boldsymbol{\beta}}_1\cdot\boldsymbol{n}, \boldsymbol{\tau}\cdot\boldsymbol{n}\rangle_{\partial K} &= -\langle \bar{p}_2, \boldsymbol{\tau}\cdot\boldsymbol{n}\rangle_{\partial K} + \langle \alpha_p\bar{\boldsymbol{\beta}}_2\cdot\boldsymbol{n}, \boldsymbol{\tau}\cdot\boldsymbol{n}\rangle_{\partial K}\,, &(38)\\
-\langle \bar{\boldsymbol{\beta}}_1\cdot\boldsymbol{n}, q\rangle_{\partial K} + \langle \alpha_\beta\bar{p}_1, q\rangle_{\partial K} &= -\langle \bar{\boldsymbol{\beta}}_2\cdot\boldsymbol{n}, q\rangle_{\partial K} + \langle \alpha_\beta\bar{p}_2, q\rangle_{\partial K}\,, &(39)
\end{aligned}$$

hold for any q and $\boldsymbol{\tau}$. Let us choose $\boldsymbol{\tau}\cdot\boldsymbol{n} = q$ and consider the sum of (39) and the product of α_β and (38), and, conversely, the sum of (38) and the product of α_p and (39). We obtain

$$\begin{aligned}
(\alpha_p\alpha_{\boldsymbol{\beta}} - 1)\,\langle \bar{p}_1 - \bar{p}_2\,,\, q\rangle_{\partial K} &= 0\,, &(40)\\
(\alpha_p\alpha_{\boldsymbol{\beta}} - 1)\,\langle (\bar{\boldsymbol{\beta}}_1 - \bar{\boldsymbol{\beta}}_2)\cdot\boldsymbol{n}, q\rangle_{\partial K} &= 0\,, &(41)
\end{aligned}$$

Observing that the mass matrices associated with the variational statement (40) are invertible, and using the assumption that $\alpha_p\alpha_{\boldsymbol{\beta}} \neq 1$ we conclude that $\bar{p}_1 = \bar{p}_2$, that is the degrees-of-freedom

associated with $\bar{p}_1$ and $\bar{p}_2$ coincide. Condition (41) is equivalent to $\bar{\boldsymbol{\beta}}_1 = \bar{\boldsymbol{\beta}}_2$ in the case of $\mathbb{RT}^0$ spaces, while the case in which $\bar{\boldsymbol{\beta}} \in (\mathcal{P}^1(K))^{n_d}$ is more subtle. In fact, in the latter case, condition (41), for triangular elements, produces a system of three equations in three unknown degrees of freedom for the vector $\Delta\bar{\boldsymbol{\beta}} = \bar{\boldsymbol{\beta}}_1 - \bar{\boldsymbol{\beta}}_2$, and of four equations in four unknowns in the case of tetrahedral elements in three dimensions. Due to the properties of the orientation of the outward normal in convex simplexes, these equations are solvable and lead again to $\Delta\bar{\boldsymbol{\beta}} = \mathbf{0}$. Hence we infer that $\bar{\boldsymbol{Y}}_{1;K} = \bar{\boldsymbol{Y}}_{2;K}$, which concludes the proof. □

Corollary 2. *Assume that all local transfer operators T_K with $K \in \mathcal{T}_h$ are injective. Then global transfer operator $T_\Omega = \mathsf{A}_{K\in\mathcal{T}_h} T_K$ is injective.*

Proof. By contradiction: Assume that T_Ω is not injective, then, by the way it is constructed, there must be a $K \in \mathcal{T}_h$ such that its corresponding T_K is not injective, which is a contradiction. □

Proposition 6 (Consistency)**.** *If the DG formulation is consistent, then the corresponding DSDG formulation is consistent, that is, $\forall\,(\boldsymbol{\tau}, q) \in R(T_\Omega^0)$, $B(\boldsymbol{\beta}_e - \boldsymbol{\beta}, p_e - p; \tau, p) = 0$.*

Proof. This is a direct consequence that the base DG formulation is consistent, since $R(T_\Omega^0)$ is a proper subspace of the base DG space $\boldsymbol{M}_d$. □

Proposition 7 (Consistency of the local problem)**.** *The exact solution $(\boldsymbol{\beta}_e, p_e)$ to (1) satisfies the local problem (9a)-(9b) on each element and the boundary conditions.*

Proof. Since $(\boldsymbol{\beta}_e, p_e)$ is the exact solution, then on each element we have

$$(\boldsymbol{\Lambda}^{-1}\boldsymbol{\beta}_e + \nabla p_e, \tau)_K = 0 \tag{42}$$

$$(\nabla \cdot \boldsymbol{\beta}_e, q)_K = (\phi, q)_K \tag{43}$$

Integrating by parts, and adding and subtracting $\langle \boldsymbol{\beta}_e \cdot \boldsymbol{n}, q\rangle_{\partial\Omega}$, we derive

$$(\boldsymbol{\Lambda}^{-1}\boldsymbol{\beta}_e, \boldsymbol{\tau})_K - (p_e, \nabla \cdot \boldsymbol{\tau})_K + \langle p_e, \boldsymbol{\tau} \cdot n\rangle_{\partial K} = 0 \tag{44}$$

$$(\nabla \cdot \boldsymbol{\beta}_e, q)_K - \langle \boldsymbol{\beta}_e \cdot \boldsymbol{n}, q\rangle_{\partial K} + \langle \boldsymbol{\beta}_e \cdot \boldsymbol{n}, q\rangle_{\partial K} = (\phi, q)_K \tag{45}$$

Substituting $\boldsymbol{\beta} = \bar{\boldsymbol{\beta}} = \boldsymbol{\beta}_e$, $p = \bar{p} = p_e$ into (10)-(11), we get $\hat{p} = p_e$, $\hat{\boldsymbol{\beta}} = \boldsymbol{\beta}_e$. Hence, identifying $\hat{p} = p_e$ and $\hat{\boldsymbol{\beta}} = \boldsymbol{\beta}_e$, we have

$$(\boldsymbol{\Lambda}^{-1}\boldsymbol{\beta}_e, \boldsymbol{\tau})_K - (p_e, \nabla \cdot \boldsymbol{\tau})_K + \langle \hat{p}, \boldsymbol{\tau} \cdot n\rangle_{\partial K} = 0 \tag{46}$$

$$(\nabla \cdot \boldsymbol{\beta}_e, q)_K - \langle \boldsymbol{\beta}_e \cdot \boldsymbol{n}, q\rangle_{\partial K} + \langle \hat{\boldsymbol{\beta}} \cdot \boldsymbol{n}, q\rangle_{\partial K} = (\phi, q)_K \tag{47}$$

Hence, the exact solution $(\boldsymbol{\beta}_e, p_e)$ satisfies the local problem. If we rewrite the local problem as $B_{\text{loc}}(\boldsymbol{\beta}, p; \boldsymbol{\tau}, q) = L_{\text{loc}}(\boldsymbol{\tau}, q)$, then we have $\forall\,(\boldsymbol{\tau}, q) \in \boldsymbol{M}_d(K)$

$$B_{\text{loc}}(\boldsymbol{\beta}_e - \boldsymbol{\beta}, p_e - p; \boldsymbol{\tau}, q) = L_{\text{loc}}(\boldsymbol{\tau}, q) \quad \text{(Galerkin othogonality)}$$

□

Corollary 3 (Fixed point property)**.** *For any constant c, $(\boldsymbol{\beta} = 0, p = c)$ is a fixed point for the homogeneous part T_K^0 of the local transfer operator, and also the homogenous part T_Ω^0 of the global transfer operator.*

Proof. First, observe that $(\boldsymbol{\beta} = 0, p = c)$ is an exact solution to the global problem (with zero source term and constant Dirichlet Boundary condition equal to c). Proposition 7 implies that $(\boldsymbol{\beta} = 0, p = c)$ is also solution to the local problem by setting $\bar{\boldsymbol{\beta}} = \boldsymbol{\beta} = 0, \bar{p} = p = c$ and $\phi = 0$.

Now, $(\boldsymbol{\beta} = 0, p = c) \in \boldsymbol{M}_c$, which means $(\boldsymbol{\beta} = 0, p = c)$ can exactly be expressed by shape functions either in $\boldsymbol{M}_c$ or $\boldsymbol{M}_d$. Applying the definition of local transfer operator (14a)-(14b) on each element, we can derive that the degrees-of-freedom satisfy $\boldsymbol{Y}_K = \bar{\boldsymbol{Y}}_K = [\boldsymbol{0}, \boldsymbol{c}]^T$. Therefore, $(\boldsymbol{\beta} = 0, p = c)$ is a fixed point of the homogenous local transfer operator.

Summing the previous results over all the elements, $(\boldsymbol{\beta} = 0, p = c)$ maps to itself through the global homogeneous transfer operator T^0_Ω. Hence it is a fixed point of T^0_Ω. □

8.1 Stability (existence and uniqueness of the solution) for the global problem

Theorem 1 (Inf-sup condition)**.** *For any $(\boldsymbol{\beta}, p) \in R(T^0_\Omega)$, there exists a constant $c > 0$, such that*

$$c\,|||\boldsymbol{\beta}, p||| \leq \sup_{(\boldsymbol{\tau},q)\in R(T)} \frac{B\left(\boldsymbol{\beta}, p; \boldsymbol{\tau}, q\right)}{|||\boldsymbol{\tau}, q|||}\,,$$

where

$$|||\boldsymbol{\beta}, p|||^2 = \|\boldsymbol{\Lambda}^{-1/2}\boldsymbol{\beta}\|^2_\Omega + \|\boldsymbol{\Lambda}^{1/2}\nabla p\|^2_\Omega + \|(h^\perp)^{-1/2}\|\boldsymbol{\Lambda}\|^{1/2}[\![p]\!]\|^2_{\mathcal{E}\setminus\Gamma_N}\,.$$

Proof. The theorem can be equivalently stated as: $\forall\,(\boldsymbol{\beta}, p) \in R(T^0_\Omega)$, there exists a constant $c > 0$ and $(\boldsymbol{\beta}', p') \in R(T^0_\Omega)$, such that

$$c\,|||\boldsymbol{\beta}, p||| \leq \frac{B(\boldsymbol{\beta}, p; \boldsymbol{\beta}', p')}{|||\boldsymbol{\beta}', p'|||}\,.$$

In what follow, we are adapting to the DSDG setting the proof developed in [12] for a standard DG method. We will also need the following

Lemma 1 (Trace inequality)**.** *$\forall \boldsymbol{\tau} \in \boldsymbol{V}^d$, $\exists c_T \in \mathbb{R}^+$, independent of the mesh size, such that*

$$\|\,\{\boldsymbol{\tau}\}\,\|^2_{\mathcal{E}\setminus\Gamma_N} + \|[\![\boldsymbol{\tau}]\!]\|^2_{\mathcal{E}\setminus\Gamma_N} \leq c_T\|h^{-1/2}\boldsymbol{\tau}\|_\Omega\,.$$

On the other hand, $\forall \boldsymbol{\tau} \in (H^1(K)^d$, $\exists c_T \in \mathbb{R}^+$, independent of the mesh size, such that

$$\|\,\{\boldsymbol{\tau}\}\,\|^2_{\mathcal{E}\setminus\Gamma_N} + \|[\![\boldsymbol{\tau}]\!]\|^2_{\mathcal{E}\setminus\Gamma_N} \leq c_T\left(\|h^{-1/2}\boldsymbol{\tau}\|_\Omega + |h^{1/2}\boldsymbol{\tau}|_\Omega\right)\,.$$

Lemma 2 (Coercivity)**.** *For any $(\boldsymbol{\beta}, p) \in R(T^0_\Omega)$, there exists a positive constant c_L, such that*

$$c_L B\left(\boldsymbol{\beta}, p; \boldsymbol{\beta}, p\right) \geq \|\boldsymbol{\Lambda}^{-1/2}\boldsymbol{\beta}\|_\Omega + \|(h^\perp)^{-1/2}\|\boldsymbol{\Lambda}\|^{1/2}[\![p]\!]\|_{\mathcal{E}\setminus\Gamma_N}$$

Proof. Since $R(T^0_\Omega) \subset \boldsymbol{M}_d$, the DSDG statement of coercivity is a special case of the general statement of coercivity of Proposition 3. □

First, integrating back by parts the variational forms (6)-(7), we obtain

$$\begin{aligned}
\left(\boldsymbol{\Lambda}^{-1}\boldsymbol{\beta}, \boldsymbol{\tau}\right)_\Omega + \left(\nabla p, \boldsymbol{\tau}\right)_\Omega - \langle\{\boldsymbol{\tau}\}, [\![p]\!]\rangle_{\mathcal{E}\setminus\Gamma_N} &= 0\,,\\
-\left(\boldsymbol{\beta}, \nabla q\right)_\Omega + \langle\{\boldsymbol{\beta}\}, [\![q]\!]\rangle_{\mathcal{E}\setminus\Gamma_N} + \langle\alpha[\![p]\!], [\![q]\!]\rangle_{\mathcal{E}\setminus\Gamma_N} - \langle\alpha p_D, q\rangle_{\Gamma_D} - \langle h_N, q\rangle_{\Gamma_N} &= \left(\phi, q\right)_\Omega\,,
\end{aligned}$$

so that the DG bilinear form can be recast as:

$$\begin{aligned} B\left(\boldsymbol{\beta}, p; \boldsymbol{\tau}, q\right) = & \left(\boldsymbol{\Lambda}^{-1}\boldsymbol{\beta}, \boldsymbol{\tau}\right)_{\Omega} + \left(\nabla p, \boldsymbol{\tau}\right)_{\Omega} - \langle\{\boldsymbol{\tau}\}, [\![p]\!]\rangle_{\mathcal{E}\setminus\Gamma_N} - \left(\boldsymbol{\beta}, \nabla q\right)_{\Omega} \\ & + \langle\{\boldsymbol{\beta}\}, [\![q]\!]\rangle_{\mathcal{E}\setminus\Gamma_N} + \langle\alpha[\![p]\!], [\![q]\!]\rangle_{\mathcal{E}\setminus\Gamma_N} . \end{aligned} \tag{48}$$

By the definition of the bilinear form, we can write

$$\|\boldsymbol{\Lambda}^{1/2}\nabla p\|_{\Omega}^2 \;\; = \;\; B\left(\boldsymbol{\beta}, p; \boldsymbol{\Lambda}\nabla p, 0\right) - \left(\boldsymbol{\beta}, \nabla p\right)_{\Omega} + \langle\{\boldsymbol{\Lambda}\nabla p\}, [\![p]\!]\rangle_{\mathcal{E}\setminus\Gamma_N} , \tag{49}$$

The third term in (49) can be bound using Young's inequality (i.e., the ϵ-inequality with $\epsilon = 2$):

$$|\left(\boldsymbol{\beta}, \nabla p\right)_{\Omega}| \leq \frac{1}{2\epsilon_1}\|\boldsymbol{\Lambda}^{-1/2}\boldsymbol{\beta}\|_{\Omega}^2 + \frac{\epsilon_1}{2}\|\boldsymbol{\Lambda}^{1/2}\nabla p\|_{\Omega}^2 . \tag{50}$$

Choosing $\boldsymbol{\tau} = h^{1/2}\boldsymbol{\Lambda}\nabla p$ in Lemma 1, we derive

$$\|h^{1/2}\{\boldsymbol{\Lambda}\nabla p\}\|_{\mathcal{E}\setminus\Gamma_N}^2 \leq \|h^{1/2}\{\boldsymbol{\Lambda}\nabla p\}\|_{\mathcal{E}\setminus\Gamma_N}^2 + \|h^{1/2}[\![\boldsymbol{\Lambda}\nabla p]\!]\|_{\mathcal{E}\setminus\Gamma_N}^2 \leq c_T\|\boldsymbol{\Lambda}\nabla p\|_{\Omega}^2 .$$

The last term in (49) can be bound using, in sequence, Young's inequality, the trace inequality, and the Cauchy-Schwartz inequality:

$$\begin{aligned} \left|\langle\{\boldsymbol{\Lambda}\nabla p\}, [\![p]\!]\rangle_{\mathcal{E}\setminus\Gamma_N}\right| \leq & \;\frac{c_T}{2\epsilon_2}\|(h^{\perp})^{-1/2}\|\boldsymbol{\Lambda}^{1/2}\|\,[\![p]\!]\|_{\mathcal{E}\setminus\Gamma_N}^2 + \frac{\xi_2}{4c_T}\|h^{1/2}\|\boldsymbol{\Lambda}^{1/2}\|^{-1}\{\boldsymbol{\Lambda}\nabla p\}\|_{\mathcal{E}\setminus\Gamma_N}^2 \\ \leq & \;\frac{c_T}{2\epsilon_2}\|(h^{\perp})^{-1/2}\|\boldsymbol{\Lambda}^{1/2}\|\,[\![p]\!]\|_{\mathcal{E}\setminus\Gamma_N}^2 + \frac{\epsilon_2\xi_2}{2}\|\|\boldsymbol{\Lambda}^{1/2}\|^{-1}\boldsymbol{\Lambda}\nabla p\|_{\Omega}^2 \\ \leq & \;\frac{c_T}{2\epsilon_2}\|(h^{\perp})^{-1/2}\|\boldsymbol{\Lambda}^{1/2}\|\,[\![p]\!]\|_{\mathcal{E}\setminus\Gamma_N}^2 + \frac{\epsilon_2\xi_2}{2}\|(\|\boldsymbol{\Lambda}^{1/2}\|^{-1}\boldsymbol{\Lambda}^{1/2})\boldsymbol{\Lambda}^{1/2}\nabla p\|_{\Omega}^2 \\ \leq & \;\frac{c_T}{2\epsilon_2}\|(h^{\perp})^{-1/2}\|\boldsymbol{\Lambda}^{1/2}\|\,[\![p]\!]\|_{\mathcal{E}\setminus\Gamma_N}^2 + \frac{\epsilon_2\xi_2\tilde{C}}{2}\|\boldsymbol{\Lambda}^{1/2}\nabla p\|_{\Omega}^2 , \end{aligned}$$

where ξ_2 is found in (2) and the $\tilde{C} \in \mathbb{R}^+$ is such that $\forall\boldsymbol{\tau},\ \|(\|\boldsymbol{\Lambda}^{1/2}\|^{-1}\boldsymbol{\Lambda}^{1/2})\boldsymbol{\tau}\|_{\Omega}^2 \leq \tilde{C}\|\boldsymbol{\tau}\|_{\Omega}^2$. Combining all these bounds, we have

$$\|\boldsymbol{\Lambda}^{1/2}\nabla p\|_{\Omega}^2 \leq B(\boldsymbol{\beta}, p; \tilde{C}_1\boldsymbol{\Lambda}\nabla p, 0) + \tilde{C}_2\|\boldsymbol{\Lambda}^{-1/2}\boldsymbol{\beta}\|_{\Omega}^2 + \tilde{C}_3\|(h^{\perp})^{-1/2}\|\boldsymbol{\Lambda}^{1/2}\|\,[\![p]\!]\|_{\mathcal{E}\setminus\Gamma_N}^2 .$$

where for ϵ_1 and ϵ_2 sufficiently small:

$$\tilde{C}_1 = \left(1 - \frac{\epsilon_1}{2} - \frac{\epsilon_2\xi_2\tilde{C}}{2}\right)^{-1}, \qquad \tilde{C}_2 = \frac{\tilde{C}_1}{2\epsilon_1}, \qquad \tilde{C}_3 = \frac{c_T\tilde{C}_1}{2\epsilon_2}$$

From the definition of the triple norm, we have

$$\begin{aligned} |||(\boldsymbol{\beta}, p)|||^2 = & \;\|\boldsymbol{\Lambda}^{-1/2}\boldsymbol{\beta}\|_{\Omega}^2 + \|\boldsymbol{\Lambda}^{1/2}\nabla p\|_{\Omega}^2 + \|(h^{\perp})^{-1/2}\|\boldsymbol{\Lambda}^{1/2}\|\,[\![p]\!]\|_{\mathcal{E}\setminus\Gamma_N}^2 \\ \leq & \;(1+\tilde{C}_2)\|\boldsymbol{\Lambda}^{-1/2}\boldsymbol{\beta}\|_{\Omega}^2 + B(\boldsymbol{\beta}, p; \tilde{C}_1\boldsymbol{\Lambda}\nabla p, 0) + (1+\tilde{C}_3)\|(h^{\perp})^{-1/2}\|\boldsymbol{\Lambda}^{1/2}\|\,[\![p]\!]\|_{\mathcal{E}\setminus\Gamma_N}^2 \\ \leq & \;B\left(\boldsymbol{\beta}, p; \tilde{C}_1\boldsymbol{\Lambda}\nabla p, 0\right) + (1+\max\{\tilde{C}_2, \tilde{C}_3\})B\left(\boldsymbol{\beta}, p; \boldsymbol{\beta}, p\right) \\ \leq & \;B\left(\boldsymbol{\beta}, p; \boldsymbol{\beta}', p'\right), \end{aligned} \tag{51}$$

where

$$\begin{aligned}\boldsymbol{\beta}' &= \tilde{C}_1 \boldsymbol{\Lambda} \nabla p + \gamma \boldsymbol{\beta}\,,\\ p' &= \gamma p\,,\\ \gamma &= 1 + \max\{\tilde{C}_2, \tilde{C}_3\}\,,\end{aligned}$$

and $(\boldsymbol{\beta}', p') \in R(T_\Omega^0)$, by the following

Lemma 3. *For any $q \in R(T_\Omega^0) \bigcap \mathcal{P}^1(\Omega)$, there exist $\boldsymbol{\tau} = \boldsymbol{\Lambda}\nabla q$ in $R(T_\Omega^0) \bigcap \mathcal{P}^0(\Omega)$.*

Proof. First observe that $\boldsymbol{\Lambda}\nabla q$ is constant on each of the elements of the mesh discretization since $q \in R(T_\Omega^0) \bigcap \mathcal{P}^1(\Omega)$. Applying Corollary 3, we also know that a piecewise constant vector field is a fixed point of the homogenous transfer operator for the flux. Then it follows that $\boldsymbol{\tau} = \boldsymbol{\Lambda}\nabla q$. □

By the definition of triple norm and Young's inequality (50), we have

$$\begin{aligned}|||\boldsymbol{\beta}', p'|||^2 &= \|\boldsymbol{\Lambda}^{-1/2}\boldsymbol{\beta}'\|_\Omega^2 + \|\boldsymbol{\Lambda}^{1/2}\nabla p'\|_\Omega^2 + \|(h^\perp)^{-1/2}\,\|\boldsymbol{\Lambda}^{1/2}\|[\![p']\!]\|_{\mathcal{E}\setminus\Gamma_N}^2\\ &= \|\boldsymbol{\Lambda}^{-1/2}(\tilde{C}_1\boldsymbol{\Lambda}\nabla p + \gamma\boldsymbol{\beta})\|_\Omega^2 + \gamma^2\|\boldsymbol{\Lambda}^{1/2}\nabla p\|_\Omega^2 + \|\gamma h^\perp)^{-1/2}\,\|\boldsymbol{\Lambda}^{1/2}\|[\![p]\!]\|_{\mathcal{E}\setminus\Gamma_N}^2\\ &= \tilde{C}_1^2\|\boldsymbol{\Lambda}^{1/2}\nabla p\|_\Omega^2 + \gamma^2\|\boldsymbol{\Lambda}^{-1/2}\boldsymbol{\beta}\|_\Omega^2 + 2\tilde{C}_1\gamma(\nabla p, \boldsymbol{\beta})_\Omega + \gamma^2\|\boldsymbol{\Lambda}^{1/2}\nabla p\|_\Omega^2\\ &\quad + \gamma^2\|h^\perp)^{-1/2}\,\|\boldsymbol{\Lambda}^{1/2}\|[\![p]\!]\|_{\mathcal{E}\setminus\Gamma_N}^2\\ &\le (\tilde{C}_1^2 + \tilde{C}_1\gamma + \gamma^2)\|\boldsymbol{\Lambda}^{1/2}\nabla p\|_\Omega^2 + (\tilde{C}_1\gamma + \gamma^2)\|\boldsymbol{\Lambda}^{-1/2}\boldsymbol{\beta}\|_\Omega^2 + \gamma^2\|h^\perp)^{-1/2}\,\|\boldsymbol{\Lambda}^{1/2}\|[\![p]\!]\|_{\mathcal{E}\setminus\Gamma_N}^2\\ &\le (\tilde{C}_1^2 + \tilde{C}_1\gamma + \gamma^2)\,|||\boldsymbol{\beta}, p|||^2\end{aligned}$$

Combining this result with (51), we have

$$B\left(\boldsymbol{\beta}, p; \boldsymbol{\beta}', p'\right) \ge |||\boldsymbol{\beta}, p|||^2 \ge c\,|||\boldsymbol{\beta}, p|||\;|||\boldsymbol{\beta}', p'|||\,, \tag{52}$$

that is

$$c\,|||\boldsymbol{\beta}, p||| \le \frac{B\left(\boldsymbol{\beta}, p; \boldsymbol{\beta}', p'\right)}{|||\boldsymbol{\beta}', p'|||} \tag{53}$$

with $c = \sqrt{\tilde{C}_1^2 + \tilde{C}_1\gamma + \gamma^2}$ and $(\boldsymbol{\beta}, p) \in R\left(T_\Omega^0\right)$. □

8.2 Continuity

Proposition 8. *The bilinear form $B\left(\boldsymbol{\beta}, p; \boldsymbol{\tau}, q\right)$ is continuous in the norm $|||\cdot,\cdot|||$,*

$$B\left(\boldsymbol{\beta}, p; \boldsymbol{\tau}, q\right) \le c\,|||\boldsymbol{\beta}, p|||\;|||\boldsymbol{\tau}, q|||\,. \tag{54}$$

Proof. Let us first recall the definition of the bilinear form from (8), and integrate by parts the inter-element boundary terms:

$$\begin{aligned}B(\boldsymbol{\beta}, p; \boldsymbol{\tau}, q) = {} & (\boldsymbol{\Lambda}^{-1}\boldsymbol{\beta}, \boldsymbol{\tau})_\Omega + (\nabla p, \boldsymbol{\tau})_\Omega - \langle\{\boldsymbol{\tau}\}, [\![p]\!]\rangle_{\mathcal{E}\setminus\Gamma_N}\\ & (\boldsymbol{\beta}, \nabla q) - \langle\{\beta\}, [\![q]\!]\rangle_{\mathcal{E}\setminus\Gamma_N} - \langle[\![q]\!], \alpha\,[\![p]\!]\rangle_{\mathcal{E}_i} - \langle q, \alpha\, p\rangle_{\Gamma_D}\,.\end{aligned} \tag{55}$$

All the terms in the bilinear form can be bounded using the Cauchy-Schwartz and trace inequalities. Namely:

$$\begin{aligned}
\left(\boldsymbol{\Lambda}^{-1}\boldsymbol{\beta},\boldsymbol{\tau}\right)_{\Omega} &\leq \|\boldsymbol{\Lambda}^{-1/2}\boldsymbol{\beta}\|_{\Omega}\,\|\boldsymbol{\Lambda}^{-1/2}\boldsymbol{\tau}\|_{\Omega} \leq |||\boldsymbol{\beta},p|||\,|||\boldsymbol{\tau},q||| \\
(\nabla p,\boldsymbol{\tau})_{\Omega} &\leq \|\boldsymbol{\Lambda}^{1/2}\nabla p\|\,\|\boldsymbol{\Lambda}^{-1/2}\boldsymbol{\tau}\| \leq |||\boldsymbol{\beta},p|||\,|||\boldsymbol{\tau},q||| \\
(\nabla q,\boldsymbol{\beta})_{\Omega} &\leq \|\boldsymbol{\Lambda}^{1/2}\nabla q\|\,\|\boldsymbol{\Lambda}^{-1/2}\boldsymbol{\beta}\| \leq |||\boldsymbol{\beta},p|||\,|||\boldsymbol{\tau},q|||
\end{aligned}$$

and

$$\begin{aligned}
\langle\{\boldsymbol{\tau}\},[\![p]\!]\rangle_{\mathcal{E}\setminus\Gamma_N} &\leq \xi_2\|h^{1/2}\,\|\boldsymbol{\Lambda}\|^{-1/2}\,\{\boldsymbol{\tau}\}\,\|_{\mathcal{E}\setminus\Gamma_N}\|(h^{\perp})^{-1/2}\,\|\boldsymbol{\Lambda}\|^{1/2}[\![p]\!]\|_{\mathcal{E}\setminus\Gamma_N} \\
&\leq \xi_2\tilde{C}c_T\|\boldsymbol{\Lambda}^{-1/2}\boldsymbol{\tau}\|_{\Omega}\,\|h^{-1/2}\|\boldsymbol{\Lambda}\|^{1/2}[\![p]\!]\|_{\mathcal{E}\setminus\Gamma_N} \\
&\leq c\,|||\boldsymbol{\beta},p|||\,|||\boldsymbol{\tau},q||| \\
\langle\{\boldsymbol{\beta}\},[\![q]\!]\rangle_{\mathcal{E}\setminus\Gamma_N} &\leq c\,|||\boldsymbol{\beta},p|||\,|||\boldsymbol{\tau},q||| \\
\langle\alpha[\![p]\!],[\![q]\!]\rangle_{\mathcal{E}\setminus\Gamma_N} &\leq c\|h^{1/2}\,\{\boldsymbol{\Lambda}\}^{1/2}\,[\![p]\!]\|_{\mathcal{E}\setminus\Gamma_N}\|h^{1/2}\,\{\boldsymbol{\Lambda}\}^{1/2}\,[\![q]\!]\|_{\mathcal{E}\setminus\Gamma_N} \leq c\,|||\boldsymbol{\beta},p|||\,|||\boldsymbol{\tau},q|||\,.
\end{aligned}$$

Combining all these results, we conclude the proof. □

8.3 Convergence

Proposition 9 (L^2-projection error)**.** *Assume the analytical solution $\boldsymbol{\beta} \in (H^{r_{\boldsymbol{\beta}}})$ and $p \in H^{r_p}$, then the L^2-projection π_h error satisfies*

$$\begin{aligned}
\|\pi_h\boldsymbol{\beta}-\boldsymbol{\beta}\|_k &\leq\ ch^{s_{\boldsymbol{\beta}}-k}\,|\boldsymbol{\beta}|_{s_{\boldsymbol{\beta}}}\,, \\
\|\pi_h p-p\|_k &\leq\ ch^{s_p-k}\,|p|_{s_p}\,,
\end{aligned}$$

where $0 \leq s_\beta \leq \min\left(p_\beta+1, r_{\boldsymbol{\beta}}\right)$ and $0 \leq s_p \leq (p_p+1, r)$.

Proof. See for example [12] and references therein. □

The solution error in $\boldsymbol{\beta}$ and p can be decomposed as the sum of the error between the exact solution and its corresponding L^2-projection and the error between the L^2-projection of the exact solution and the numerically computed solution. Namely

$$\begin{aligned}
\boldsymbol{\beta}-\boldsymbol{\beta}_h &=\ \boldsymbol{\eta}_{\boldsymbol{\beta}}+\boldsymbol{e}_{\boldsymbol{\beta}}\,, \\
p-p_h &=\ \eta_p+e_p\,,
\end{aligned}$$

where

$$\begin{aligned}
\boldsymbol{\eta}_{\boldsymbol{\beta}} &=\ \boldsymbol{\beta}-\pi_h\boldsymbol{\beta}\,, \\
\eta_p &=\ p-\pi_h p\,,
\end{aligned}$$

and

$$\begin{aligned}
\boldsymbol{e}_{\boldsymbol{\beta}} &=\ \pi_h\boldsymbol{\beta}-\boldsymbol{\beta}_h\,, \\
e_p &=\ \pi_h p-p_h\,.
\end{aligned}$$

Theorem 2. *(Convergence) Assume the analytical solution $\boldsymbol{\beta} \in (H^{r_{\boldsymbol{\beta}}})$ and $p \in H^{r_p}$, then the error norm satisfies*

$$|||\boldsymbol{\beta} - \boldsymbol{\beta}_h, p - p_h||| \leq c\left(h^{s_{\boldsymbol{\beta}}} |\boldsymbol{\beta}|_{s_{\boldsymbol{\beta}}} + h^{s_p} |p|_{s_p}\right) ,$$

where $0 \leq s_\beta \leq \min(p_\beta + 1, r_{\boldsymbol{\beta}})$ and $0 \leq s_p \leq (p_p + 1, r)$.

Proof. From Proposition 9, we have

$$\begin{aligned}
\|\boldsymbol{\eta}_{\boldsymbol{\beta}}\| &\leq ch^{s_{\boldsymbol{\beta}}} |\boldsymbol{\beta}|_{s_{\boldsymbol{\beta}}} , \\
\left|\boldsymbol{\eta}_{\boldsymbol{\beta}}\right| &\leq ch^{s_{\boldsymbol{\beta}}-1} |\boldsymbol{\beta}|_{s_{\boldsymbol{\beta}}} , \\
\|\eta_p\| &\leq ch^{s_p} |p|_{s_p} , \\
|\eta_p| &\leq ch^{s_p-1} |p|_{s_p} .
\end{aligned}$$

Using the trace inequality (Lemma 1) and classical arguments (see also [12] for more details), it is not difficult to show that

$$|||\boldsymbol{\eta}_{\boldsymbol{\beta}}, \eta_p||| \leq c\left(h^{s_{\boldsymbol{\beta}}} |\boldsymbol{\beta}|_{s_{\boldsymbol{\beta}}} + h^{s_p-1} |p|_{s_p}\right) .$$

The numerical error can be bound using the inf-sup condition and the continuity and consistency properties

$$\begin{aligned}
|||\boldsymbol{e}_{\boldsymbol{\beta}}, e_p||| &\leq c \sup \frac{B(\boldsymbol{e}_{\boldsymbol{\beta}}, e_p; \boldsymbol{\tau}, q)}{|||\boldsymbol{\tau}, q|||} \\
&\leq c \sup \frac{B\left(\boldsymbol{\eta}_{\boldsymbol{\beta}}, \eta_p; \boldsymbol{\tau}, q\right)}{|||\boldsymbol{\tau}, q|||} \\
&\leq c\, |||\boldsymbol{\eta}_{\boldsymbol{\beta}}, \eta_p||| .
\end{aligned}$$

We conclude with the triangle inequality:

$$\begin{aligned}
|||\boldsymbol{\beta} - \boldsymbol{\beta}_h, p - p_h||| &\leq |||\boldsymbol{\eta}_{\boldsymbol{\beta}}, \eta_p||| + |||\boldsymbol{e}_{\boldsymbol{\beta}}, e_p||| \\
&\leq c\, |||\boldsymbol{\eta}_{\boldsymbol{\beta}}, e_p||| \\
&\leq c\left(h^{s_{\boldsymbol{\beta}}} |\boldsymbol{\beta}|_{s_{\boldsymbol{\beta}}} + h^{s_p-1} |p|_{s_p}\right) .
\end{aligned}$$

□

8.4 Conservation

Global conservation is easily proved by noticing that the constant test function is a fixed point for the global transfer operator, and using the statements of conservation already proved for the base DG method. The case of local conservation is more delicate, and will be proved using an approach that bears some similarities to [22].

Proposition 10 (Global conservation)**.** *The DSDG method is globally conservative.*

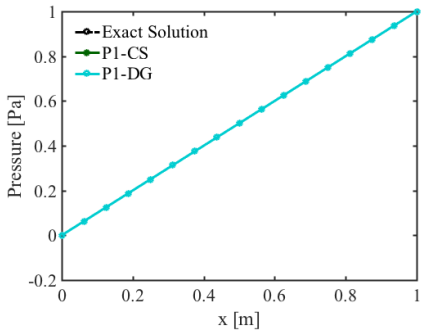

(a) Pressure.

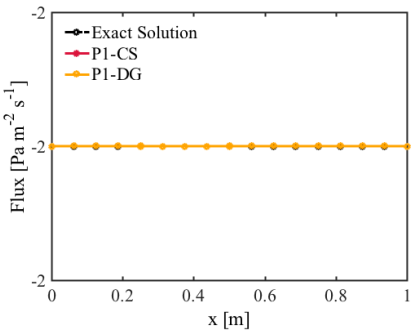

(b) Flux.

Figure 3: One-dimensional patch test on a mesh of 16 elements. $\mathcal{P}^1$-CS indicates the coarse component of the solution, while $\mathcal{P}^1$-DG indicates the post-processed discontinuous solution from the $\mathcal{P}^1$-CS component.

Proof. Substituting the test function $(\boldsymbol{\tau} = 0, q = 1) \in \boldsymbol{M}_c$ into the DSDG formulation (17) yields:

$$B\left(\boldsymbol{\beta}, p; T_\Omega^0\left(0,1\right)\right) = L\left(T_\Omega^0\left(0,1\right)\right)$$

Applying Corollary 3 on the fixed point properties of the transfer operator, we have that

$$B\left(\boldsymbol{\beta}, p; 0, 1\right) = L\left(0,1\right)$$

We conclude by applying Proposition 4, which implies that the DSDG method is globally conservative. □

Proposition 11 (Local conservation)**.** *The DSDG method is locally conservative.*

Proof. Consider a subdomain $\omega \subset \Omega$, composed of the union of adjacent elements. Consider now a test function associated with the coarse space, which is zero outside of ω, and equal to unity on a subset $\omega^o \subset \omega$ of elements that do not have any node or edge on the boundary $\partial\omega$. This test function qualitatively looks like a bump over ω. The precise shape depends on whether the space of linear polynomials $\mathbb{P}^1(K)$ or $\mathbb{RT}^0$ is used for the coarse space.

Let us assume now to enrich this test function by adding locally supported discontinuous test functions that allow to reconstruct a constant over the entire set ω. Applying similar arguments to Proposition 10, we can conclude that the fluxes built on the augmented test function space must be conservative. This argument is valid for an arbitrarily small domain ω, which may coincide with a single element, hence, with respect to the proposed construction, the DSDG method is locally conservative. □

9 Numerical tests

In the following, a number of numerical tests are performed to evaluate the performance and features of the proposed method. For comparison, the base DG method with α =2.001 will also be used.

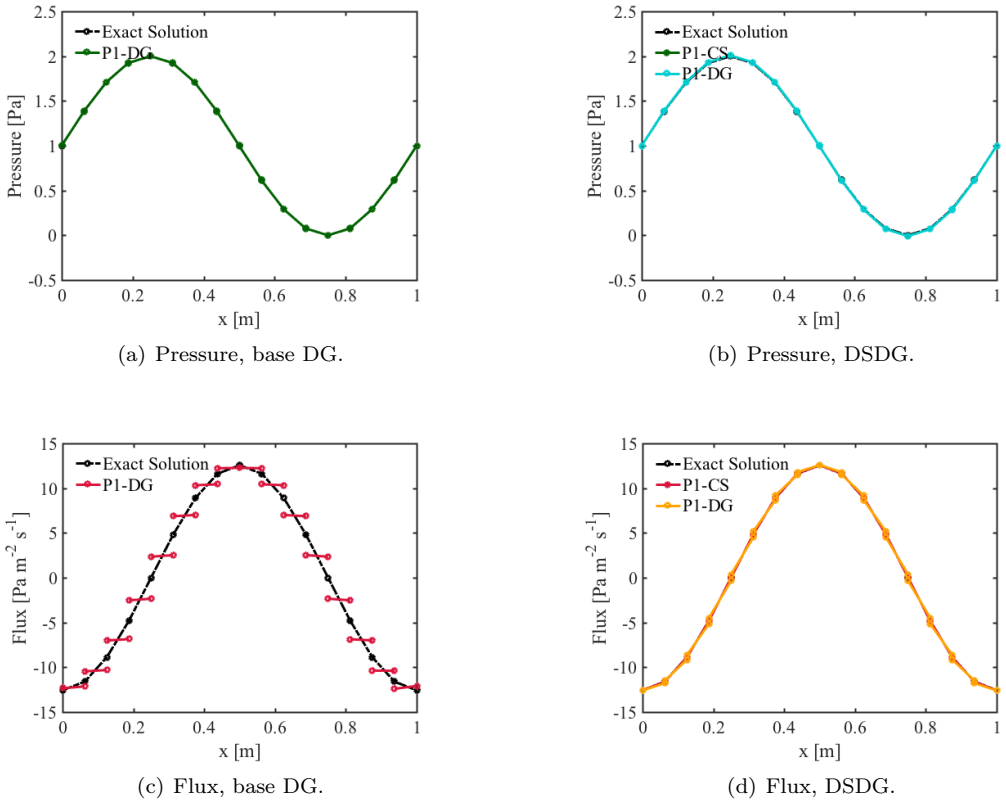

(a) Pressure, base DG.

(b) Pressure, DSDG.

(c) Flux, base DG.

(d) Flux, DSDG.

Figure 4: Smooth sinusoidal one-dimensional test on a 16-element mesh. $\mathcal{P}^1$-CS indicates the continuous component of the solution, while $\mathcal{P}^1$-DG indicates the post-processed discontinuous solution. Note the reduction of the error in flux using the DSDG method, with about half of the number of degrees-of-freedom of the original DG method.

The tests presented in what follows are chosen to highlight robustness and accuracy under smooth as well as sharp gradients and material discontinuities.

In what follows we will indicate with DSDG-$\mathbb{RT}_0$ the DSDG method in which the coarse scale space is defined by means of $\mathbb{RT}_0$ elements for the flux $\boldsymbol{\beta}$ and continuous $\mathcal{P}^1$ finite elements for the pressure p, and with DSDG-$\mathcal{P}^1$ a DSDG method, in which not only the pressure, but also the flux variables is defined by means of continuous $\mathcal{P}^1$ finite elements.

9.1 One-dimensional tests with the DSDG method

In testing the DSDG approach in one dimension, we discovered that we can safely choose $\alpha = 0$, which means there is no stabilizing penalty term for the interior interface and boundary conditions. This is somewhat surprising, since, for a DG method, this choice will produce an algebraic problem that is singular.

Our understanding is that the CS-to-DG scale transfer operator also acts as a stabilization term,

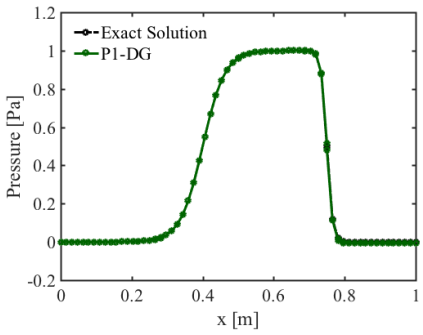

(a) Pressure, base DG.

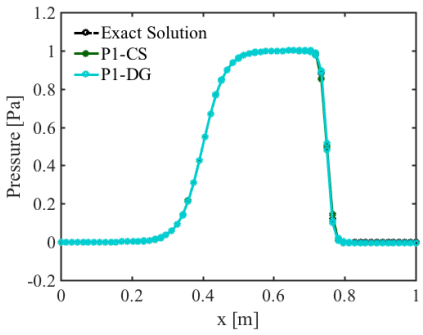

(b) Pressure, DSDG.

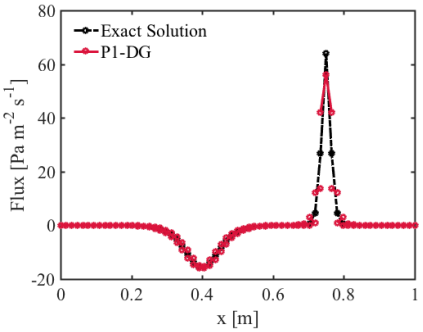

(c) Flux, based DG.

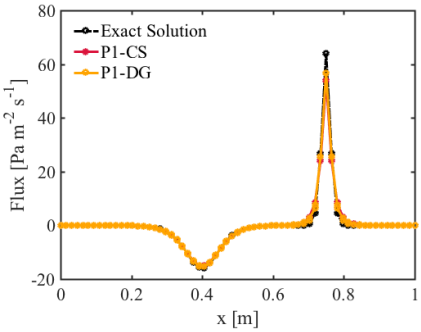

(d) Flux, DSDG.

Figure 5: Hyperbolic tangent test with sharp gradients, on a 64-element mesh. Note also in this case the reduction of the error in the case of the DSDG method, with about half of the degrees-of-freedom of the base DG method.

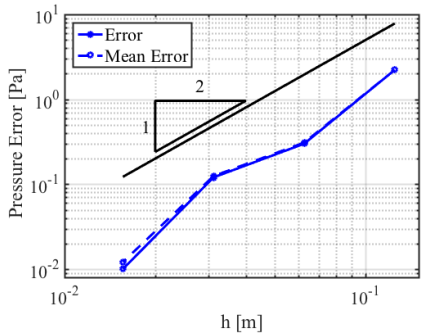

(a) Pressure, base DG.

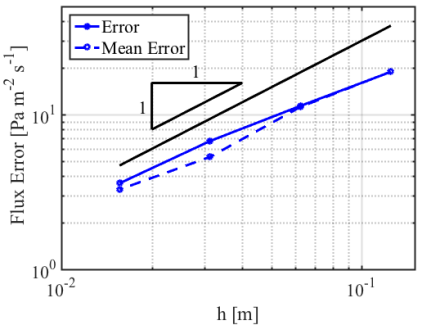

(b) Mass flux, base DG.

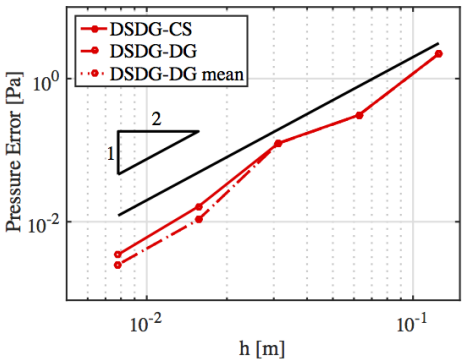

(c) Pressure, DSDG.

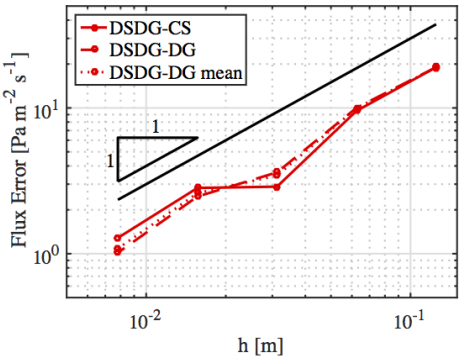

(d) Mass flux, DSDG.

Figure 6: Hyperbolic tangent test with sharp gradients: Convergence tests of the continuous component of the solution. In the bottom row plots, the L^2-norm of the error of the CS component of the DSDG solution is plotted against the L^2-norm of the post-processed discontinuous component.

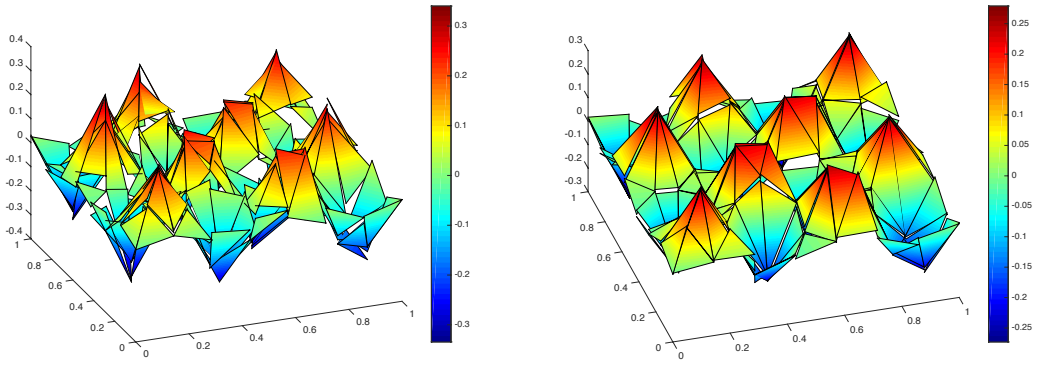

(a) Base DG.

(b) DG component post-processed from DSDG solution.

Figure 7: Smooth, periodic two-dimensional test: Pressure. The DG post-processed solution is obtained from the DSDG-$\mathbb{RT}_0$ using the local transfer map.

an aspect that warrants further investigations on our part. The penalty stabilization terms in the local transfer operator computation are chosen to be $\alpha_p = 1$ and $\alpha_\beta = 1.2$, respectively (a choice that satisfies the well-posedness discussed in Proposition 5).

9.1.1 Patch test

The first test is a consistency test for the formulation, a "sanity check." The domain is $\Omega = [0, 1]$, and the scalar mobility is $\Lambda = 2$. The mass source is zero, that is $\phi(x) = 0$, a homogenous pressure Dirichlet boundary condition, $p(0) = 0$, is applied at $x = 0$, and the Neumann condition $\beta(x) = -2$ is applied at $x = 1$. This setting leads to the exact solution

$$\begin{aligned} p(x) &= x\,, \\ \beta(x) &= -2\,, \end{aligned}$$

which, as shown in Figure 3, is correctly captured by the DSDG method, within machine precision. This test is the equivalent to a one-dimensional patch test in standard finite element formulations. We also note that Lemma 3 ensures with a mathematical proof that the proposed method satisfies a patch test. For this reason we do not show multidimensional patch tests in what follows.

9.1.2 Smooth solution test

This test involves a smooth solution and is performed on the one-dimensional domain $[0, 1]$ with mobility $\Lambda = 2$. The source term $\phi(x) = -8\pi^2 \sin(2\pi x)$, and boundary conditions $p(0) = 1$ and $\beta(1) = -4\pi$ complete the setup. The exact solution for the pressure/flux pair is:

$$p(x) = 1 + \sin(2\pi x)\,,$$

$$\beta(x) = -4\pi \cos(2\pi x)\,.$$

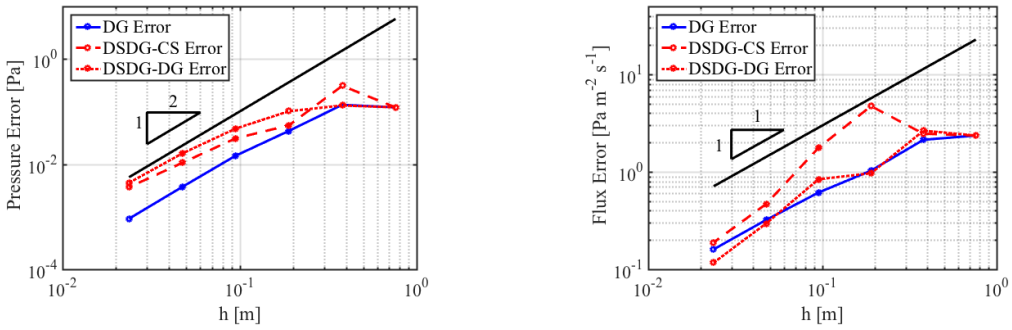

(a) Pressure. (b) Mass flux.

Figure 8: Convergence of the DSDG-$\mathbb{RT}_0$ method in the smooth periodic, two-dimensional test. Left: pressure (continuous and discontinuous components). Right: mass flux ($\mathbb{RT}_0$ and discontinuous components).

Figure 4 shows that the DSDG method captures the exact solution correctly. In particular, it is also easy to appreciate that the DSDG method is superior to the base DG method in capturing the flux $\boldsymbol{\beta}$.

9.1.3 Convergence tests for solutions with sharp gradients

A more challenging test, involving sharp gradients, is presented next. Again, $\Omega = [0, 1]$ and $\Lambda = 2$. The exact solution is given by

$$p(x) = \frac{1}{2}\tanh\left[c_1\left(x - x_1\right)\right] - \frac{1}{2}\tanh\left[c_2\left(x - x_2\right)\right] ,$$

$$\beta(x) = c_1\tanh^2\left[c_1\left(x - x_1\right)\right] - c_2\tanh^2\left[c_2\left(x - x_2\right)\right] + c_2 - c_1 ,$$

with

$$c_1 = 16,\ c_2 = 64,\ x_1 = 2/5,\ x_2 = 3/4 .$$

This solution is obtained with the method of manufactured solution, imposing an appropriate source term, not reported here for the sake of brevity, and the following Dirichlet and Neumann conditions:

$$\begin{aligned} p(0) &= 2.7608 \cdot 10^{-6} , \\ \beta(1) &= -2.9358 \cdot 10^{-7} . \end{aligned}$$

9.2 Two-dimensional tests for the DSDG-$\mathbb{RT}_0$ method

We select $\alpha = 2.001$. The penalties in the local transfer operator are $\alpha_p = 0.9$ and $\alpha_\beta = 1.0$.

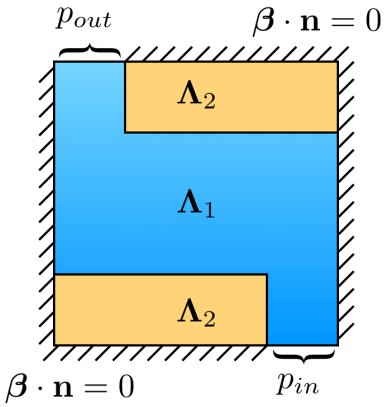

Figure 9: Geometry and material properties for the S-shaped domain test. Λ_1 and Λ_2 indicate the mobilities in different regions of the domain, with $\Lambda_1 >> \Lambda_2$.

9.3 A smooth periodic test

The first two-dimensional test to be considered is defined over the domain of unit area $\Omega = [0,1] \times [0,1]$, with $\boldsymbol{\Lambda} = \boldsymbol{I}$, with a source term

$$\phi(x,y) = 32\pi^2 \cos(2\pi x)\cos(2\pi y)\sin(2\pi x)\sin(2\pi y)\,,$$

$$\begin{aligned} p(x,y) &= \cos(2\pi x)\cos(2\pi y)\sin(2\pi x)\sin(2\pi y)\,, \\ \beta(x,y) &= \begin{bmatrix} 2\pi\sin(2\pi x)\cos(2\pi y)\sin(2\pi x)sin(2\pi y) - 2\pi\cos(2\pi x)\cos(2\pi y)\cos(2\pi x)\sin(2\pi y) \\ 2\pi\sin(2\pi y)\cos(2\pi x)\sin(2\pi x)sin(2\pi y) - 2\pi\cos(2\pi x)\cos(2\pi y)\cos(2\pi y)\sin(2\pi x) \end{bmatrix}, \end{aligned}$$

so that the exact solution for the pressure/flux pair satisfies homogenous Dirichlet boundary conditions. The solution is plotted in Figure 7, which shows that the post-processed DSDG discontinuous pressure solution closely matches the solution of the original DG method. The convergence rates, presented in Figure 8, are similar to the one-dimensional case, with the pressure being second-order accurate and the flux being first-order accurate.

9.4 S-shaped domain test

The computational domain for this test is sketched in Figure 9, and is divided into regions of different permeability (i.e., mobility). The mobility is $\boldsymbol{\Lambda}_{1,2} = \Lambda_{1,2}\boldsymbol{I}$, that is, regions indicated by the number 1 have mobility $\Lambda_1 = 100$, and regions indicated by the number 2 have mobility $\Lambda_2 = 1$. As shown in Figure 9, homogenous Neumann (flux) boundary conditions are used on the entire boundary, except the inlet and outlet, which are instead Dirichlet boundaries with the pressure set equal to 10 and 0, respectively.

The solution is computed on a grid of size $h = 0.05$. Due to the specific distribution of mobilities, the flow follows a S-shaped path inside the domain (see also Fig. 14). Figure 10 shows the pressure distribution for the $\mathbb{RT}_0$ component of the solution and the DG post-processed component of the

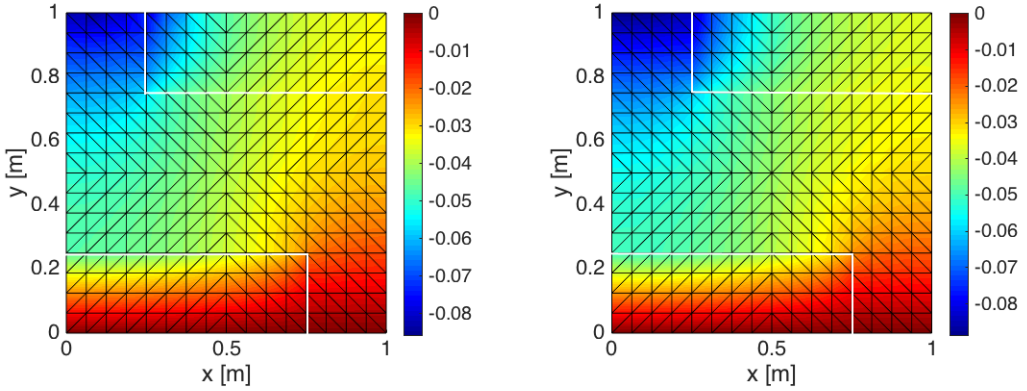

(a) $\mathbb{RT}_0$ component.

(b) Post-processed DG component.

Figure 10: S-shaped domain test: Pressure. The post-processed DG component is obtained via the DSDG local map.

solution. Figure 11 shows the x- and y-components of the mass flux. It is important to notice that the flow does not penetrate the internal corners between Region 1 and 2, avoiding a spurious feature common to numerical methods lacking physical correctness.

Figure 14 shows the flow direction and the pressure isolines: Note the mass flux vector is virtually tangent to the interfaces between Region 1 and 2. This is expected, since Region 2 has much lower permeability (flow mobility) than Region 1 and acts as a nearly impermeable layer. The S-shaped domain problem is a non-smooth test for robustness and physical accuracy of the proposed DSDG approach. It indicates that the proposed method is effective in capturing the salient physical features of the solution, even on relatively coarse grids.

9.5 Numerical Tests with the DSDG-$\mathcal{P}^1$ in two dimensions

As in the case of the DSDG-$\mathbb{RT}_0$ method, we select again $\alpha = 2.001$ for the DG penalty and $\alpha_p = 0.9$ and $\alpha_\beta = 1.0$ for the penalties in the local transfer operator.

9.6 A smooth periodic test

The domain is of unit area $\Omega = [0,1] \times [0,1]$, with $\boldsymbol{\Lambda} = \boldsymbol{I}$ and a source term

$$\phi\,(x,y) = 32\pi^2 \cos(2\pi x)\cos(2\pi y)\sin(2\pi x)\sin(2\pi y)$$

so that the exact solution for the pressure/flux pair is given by

$$p(x,y) = \cos(2\pi x)\cos(2\pi y)\sin(2\pi x)\sin(2\pi y)\,,$$

$$\beta(x,y) = \begin{bmatrix} 2\pi\sin(2\pi x)\cos(2\pi y)\sin(2\pi x)sin(2\pi y) - 2\pi\cos(2\pi x)\cos(2\pi y)\cos(2\pi x)\sin(2\pi y) \\ 2\pi\sin(2\pi y)\cos(2\pi x)\sin(2\pi x)sin(2\pi y) - 2\pi\cos(2\pi x)\cos(2\pi y)\cos(2\pi y)\sin(2\pi x) \end{bmatrix}.$$

To preserve periodicity, homogenous Dirichlet boundary conditions are imposed on the pressure. Figure (12) shows that, also in this case, the post-processed DSDG discontinuous pressure solution

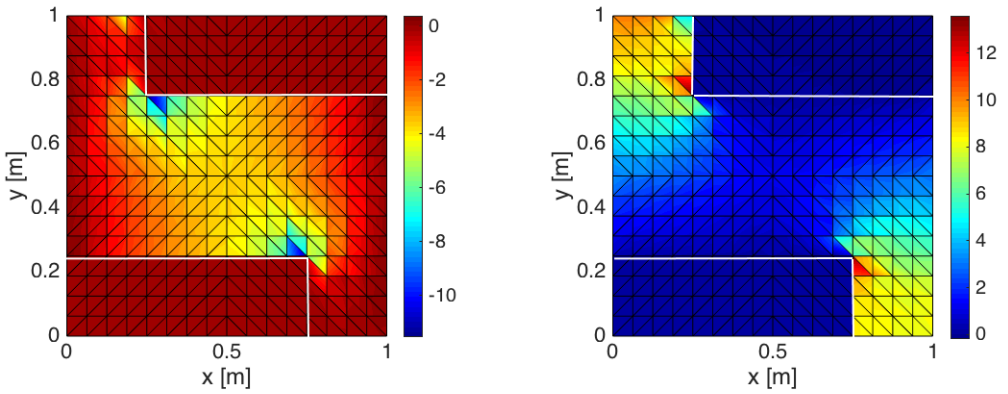

(a) Post-processed DG component in x direction.

(b) Post-processed DG component in y direction

Figure 11: S-shaped domain test: Flux. The post-processed DG component is obtained via the DSDG local map.

closely matches the solution of the original DG method. The convergence rates, presented in Figure (13), are similar to the one-dimensional case, with the pressure being second-order accurate and the flux being first-order accurate.

9.7 S-shaped domain test

Also in the case of the DSDG-$\mathcal{P}^1$ method, the solution is captured correctly for the S-shaped domain test, as shown in Figure 15.

9.8 Flow in a domain with a low permeability obstruction

A domain $\Omega = [0,1] \times [0,1]$ is divided into two regions: A center region $\Omega_c = [\frac{3}{8}, \frac{5}{8}] \times [\frac{1}{4}, \frac{3}{4}]$ with low mobility $\boldsymbol{\Lambda} = 10^{-3}\boldsymbol{I}$ and a surrounding area with higher mobility, $\boldsymbol{\Lambda} = \boldsymbol{I}$. The boundary conditions are

$$\begin{aligned} p &= 1 \quad \text{left boundary}\,, \\ p &= 0 \quad \text{right boundary}\,, \\ \boldsymbol{\beta} \cdot \boldsymbol{n} &= 0 \quad \text{elsewhere}\,. \end{aligned}$$

The mesh is obtained by splitting each of the square elements of a 40×40 grid into two triangles.

Results are shown in Figure 16, where it is easily noticed the smooth character of the flow, which bypasses the obstruction. The results of the DSDG method are actually very similar to the base DG method, with a considerable reduction in computational cost.

9.9 Random mobility

The domain geometry and boundary conditions are identical to the previous test. The mobility is $\boldsymbol{\Lambda} = \Lambda \boldsymbol{I}$, where Λ is piecewise constant on a uniform grid of 10×10 square elements and whose values

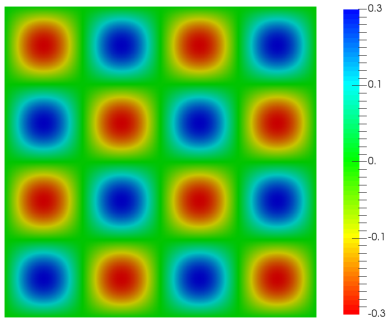

(a) Pressure, base DG.

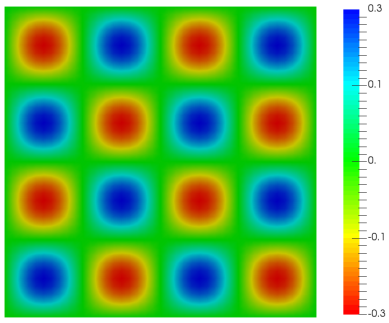

(b) Pressure, DSDG.

Figure 12: Periodic, two-dimensional smooth solution test with the DSDG-$\mathcal{P}^1$ method. Left: Pressure for the base DG method Right: The post-processed DG solution is obtained from the DSDG using the local transfer operator (17).

are generated by means of a log-normal distribution of zero mean and unit standard deviation.

The numerical results in this test involving heterogenous permeabilities are shown in Figure 17, where we observe that the DSDG and DG solutions are very similar.

9.10 A domain with a circular impermeable obstruction

The domain is again $\Omega = \Omega = [0,1] \times [0,1] \setminus \Omega_o$, where Ω_o is a circular hole with center $(0.5, 0.5)$ and radius 0.2. The boundary conditions are as in the previous two tests. The mobility is $\boldsymbol{\Lambda} = \boldsymbol{I}$ over the whole domain. Results are shown in Figure 18.

9.11 Numerical Tests for DSDG-$\mathcal{P}^1$ method in three dimensions

We again select $\alpha = 0$, and the penalties in the local transfer operator as $\alpha_p = 0.9$ and $\alpha_\beta = 1$.

9.12 Flow in a domain with a low permeability obstruction

The domain is the unit cube $\Omega = [0,1] \times [0,1] \times [0,1]$, divided into a center region $\Omega_c = [\frac{3}{8}, \frac{5}{8}] \times [\frac{1}{4}, \frac{3}{4}] \times [\frac{1}{4}, \frac{3}{4}]$ with mobility $\boldsymbol{\Lambda} = 10^{-3}\boldsymbol{I}$ and a surrounding area with mobility $\boldsymbol{\Lambda} = \boldsymbol{I}$. The boundary conditions are

$$\begin{aligned} p &= 1 \quad \text{left boundary}\,, \\ p &= 0 \quad \text{right boundary}\,, \\ \boldsymbol{\beta} \cdot \boldsymbol{n} &= 0 \quad \text{elsewhere}\,. \end{aligned}$$

The result is shown in Figure 19. Conclusions analogous to the two-dimensional case hold.

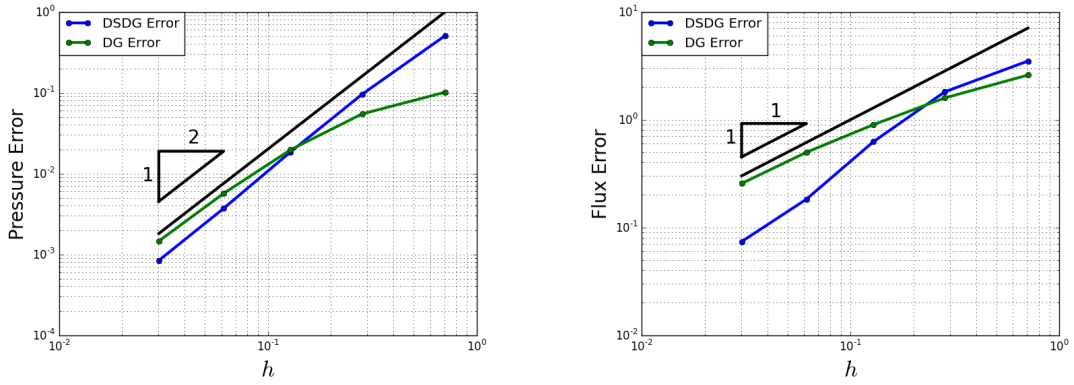

(a) DSDG-$\mathcal{P}^1$-method.

(b) Base DG method.

Figure 13: Convergence of the periodic, two-dimensional smooth solution test for the DSDG-$\mathcal{P}^1$ method.

10 Summary of main results

We have proposed a new method with computational cost analogous to continuous-type discretizations, but with performance and accuracy very similar to discontinuous Galerkin formulations. We provided stability, convergence and conservation analysis for the DSDG method by introducing a transfer operator between DG and coarse scale degrees-of-freedom. We performed extensive testing in the context of Darcy flow, demonstrating robustness, accuracy, and physical correctness of the solutions.

References

[1] Douglas N Arnold, Franco Brezzi, Bernardo Cockburn, and L Donatella Marini. Unified analysis of discontinuous galerkin methods for elliptic problems. *SIAM journal on numerical analysis*, 39(5):1749–1779, 2002.

[2] Francesco Bassi and Stefano Rebay. A high-order accurate discontinuous finite element method for the numerical solution of the compressible navier–stokes equations. *Journal of computational physics*, 131(2):267–279, 1997.

[3] Pavel Bochev, Thomas JR Hughes, and Guglielmo Scovazzi. A multiscale discontinuous galerkin method. In *Large-Scale Scientific Computing*, pages 84–93. Springer, 2005.

[4] Daniele Boffi, Nicola Cavallini, F Gardini, and Lucia Gastaldi. Local mass conservation of stokes finite elements. *Journal of scientific computing*, 52(2):383–400, 2012.

[5] Franco Brezzi, Jim Douglas Jr, Michel Fortin, and L Donatella Marini. Efficient rectangular mixed finite elements in two and three space variables. *RAIRO-Modélisation mathématique et analyse numérique*, 21(4):581–604, 1987.

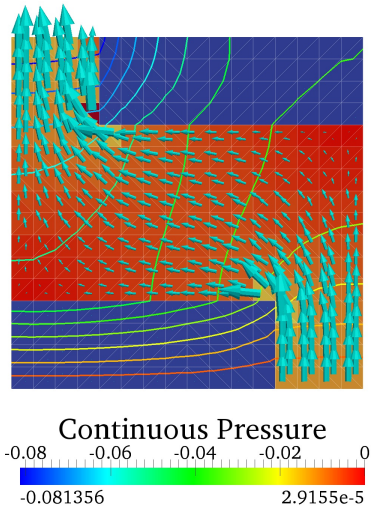

Figure 14: S-shaped domain test: Flow vectors and pressure isolines.

[6] Franco Brezzi, Jim Douglas Jr, and L Donatella Marini. Two families of mixed finite elements for second order elliptic problems. *Numerische Mathematik*, 47(2):217–235, 1985.

[7] Franco Brezzi, Thomas JR Hughes, L Donatella Marini, and Arif Masud. Mixed discontinuous galerkin methods for darcy flow. *Journal of Scientific Computing*, 22(1-3):119–145, 2005.

[8] Franco Brezzi, Gianmarco Manzini, Donatella Marini, Paola Pietra, and Alessandro Russo. Discontinuous finite elements for diffusion problems. *Francesco Brioschi (1824-1897) Convegno di Studi Matematici*, pages 197–217, 1999.

[9] Franco Brezzi, Gianmarco Manzini, Donatella Marini, Paola Pietra, and Alessandro Russo. Discontinuous galerkin approximations for elliptic problems. *Numerical Methods for Partial Differential Equations*, 16(4):365–378, 2000.

[10] William L Briggs, Steve F McCormick, et al. *A multigrid tutorial*. Siam, 2000.

[11] A Buffa, TJR Hughes, and G Sangalli. Analysis of a multiscale discontinuous galerkin method for convection-diffusion problems. *SIAM Journal on Numerical Analysis*, 44(4):1420–1440, 2006.

[12] E Burman and B Stamm. Local discontinuous galerkin method with reduced stabilization for diffusion equations. *Communications in Computational Physics*, 5:498–524, 2009.

[13] Zhangxin Chen and Jim Douglas Jr. Prismatic mixed finite elements for second order elliptic problems. *Calcolo*, 26(2-4):135–148, 1989.

[14] Bernardo Cockburn. Discontinuous galerkin methods for computational fluid dynamics. *Encyclopedia of Computational Mechanics*, 2004.

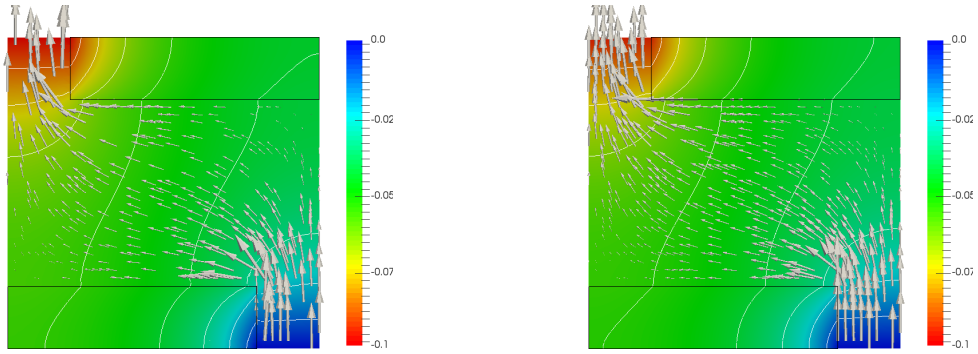

(a) DSDG method.

(b) Base DG method.

Figure 15: S-shaped domain test with the DSDG-$\mathcal{P}^1$ method: Flow vector and pressure.

[15] Bernardo Cockburn, Bo Dong, Johnny Guzmán, Marco Restelli, and Riccardo Sacco. A hybridizable discontinuous galerkin method for steady-state convection-diffusion-reaction problems. *SIAM Journal on Scientific Computing*, 31(5):3827–3846, 2009.

[16] Bernardo Cockburn, Jayadeep Gopalakrishnan, and Raytcho Lazarov. Unified hybridization of discontinuous galerkin, mixed, and continuous galerkin methods for second order elliptic problems. *SIAM Journal on Numerical Analysis*, 47(2):1319–1365, 2009.

[17] Bernardo Cockburn, Johnny Guzmán, See-Chew Soon, and Henry K Stolarski. An analysis of the embedded discontinuous galerkin method for second-order elliptic problems. *SIAM Journal on Numerical Analysis*, 47(4):2686–2707, 2009.

[18] Bernardo Cockburn, George E Karniadakis, and Chi-Wang Shu. *Discontinuous Galerkin methods: Theory, compuration and applications*. Springer, 2000.

[19] Jim Douglas Jr and Todd Dupont. Interior penalty procedures for elliptic and parabolic Galerkin methods. In *Computing methods in applied sciences*, pages 207–216. Springer, 1976.

[20] Jim Douglas Jr, Mary Fanett Wheeler, Bruce L Darlow, and Richard P Kendall. Self-adaptive finite element simulation of miscible displacement in porous media. *Computer methods in applied mechanics and engineering*, 47(1-2):131–159, 1984.

[21] H. Huang and G. Scovazzi. A high-order, fully coupled, upwind, compact discontinuous Galerkin method for modeling of viscous fingering in compressible porous media. *Computer Methods in Applied Mechanics and Engineering*, 263:169–187, 2013.

[22] Thomas JR Hughes, Gerald Engel, Luca Mazzei, and Mats G Larson. The continuous galerkin method is locally conservative. *Journal of Computational Physics*, 163(2):467–488, 2000.

[23] Thomas JR Hughes, Arif Masud, and Jing Wan. A stabilized mixed discontinuous galerkin method for darcy flow. *Computer Methods in Applied Mechanics and Engineering*, 195(25):3347–3381, 2006.

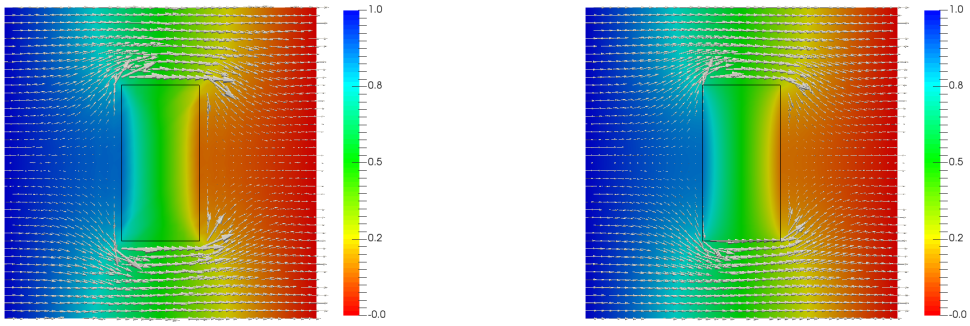

(a) DSDG method.

(b) Base DG method

Figure 16: Flow in a domain with a low permeability obstruction. The arrows represents the mass flux (velocity).

[24] Thomas JR Hughes, Guglielmo Scovazzi, Pavel B Bochev, and Annalisa Buffa. A multiscale discontinuous galerkin method with the computational structure of a continuous galerkin method. *Computer Methods in Applied Mechanics and Engineering*, 195(19):2761–2787, 2006.

[25] Sanghyun Lee, Young-Ju Lee, and Mary F Wheeler. A locally conservative enriched galerkin approximation and efficient solver for elliptic and parabolic problems. *SIAM Journal on Scientific Computing*, 38(3):A1404–A1429, 2016.

[26] Joachim Moortgat, Mohammad Amin Amooie, and Mohamad Reza Soltanian. Implicit finite volume and discontinuous galerkin methods for multicomponent flow in unstructured 3d fractured porous media. *Advances in Water Resources*, 96:389–404, 2016.

[27] Joachim Moortgat and Abbas Firoozabadi. Higher-order compositional modeling with fickian diffusion in unstructured and anisotropic media. *Advances in Water resources*, 33(9):951–968, 2010.

[28] Joachim Moortgat and Abbas Firoozabadi. Mixed-hybrid and vertex-discontinuous-galerkin finite element modeling of multiphase compositional flow on 3d unstructured grids. *Journal of Computational Physics*, 315:476–500, 2016.

[29] Joachim Moortgat, Shuyu Sun, and Abbas Firoozabadi. Compositional modeling of three-phase flow with gravity using higher-order finite element methods. *Water Resources Research*, 47(5), 2011.

[30] Jean-Claude Nédélec. Mixed finite elements in R^3. *Numerische Mathematik*, 35(3):315–341, 1980.

[31] NC Nguyen, J Peraire, and B Cockburn. Hybridizable discontinuous galerkin methods. In *Spectral and High Order Methods for Partial Differential Equations*, pages 63–84. Springer, 2011.

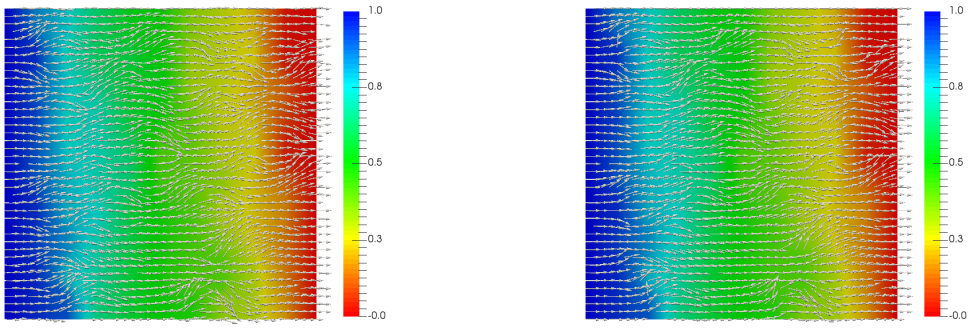

(a) DSDG method. (b) Base DG method

Figure 17: Random mobility test. The arrow represents the velocity

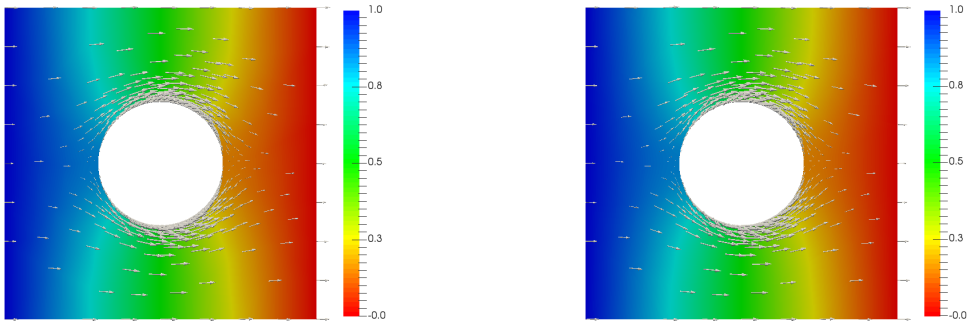

(a) DSDG method. (b) Base DG method

Figure 18: Circular impermeable obstruction mobility test. The arrow represents the velocity.

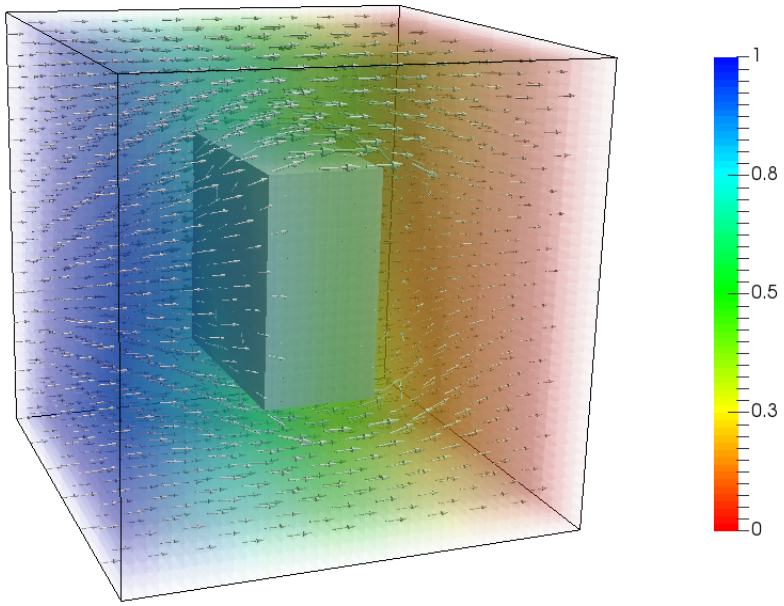

Figure 19: Test with low-permeability obstruction in three dimensions. The arrow represents the velocity

[32] Ngoc Cuong Nguyen, Jaume Peraire, and Bernardo Cockburn. An implicit high-order hybridizable discontinuous galerkin method for nonlinear convection–diffusion equations. *Journal of Computational Physics*, 228(23):8841–8855, 2009.

[33] A Quarteroni and A Valli. *Domain Decomposition Methods for Partial Differential Equations*. Numerical mathematics and scientific computation. Clarendon Press, 1999.

[34] Pierre-Arnaud Raviart and Jean-Marie Thomas. A mixed finite element method for 2-nd order elliptic problems. In *Mathematical aspects of finite element methods*, pages 292–315. Springer, 1977.

[35] Wm H Reed and TR Hill. Triangularmesh methodsfor the neutrontransportequation. *Los Alamos Report LA-UR-73-479*, 1973.

[36] G. Scovazzi, A. Gerstenberger, and S. Collis. A discontinuous Galerkin method for gravity-driven viscous fingering instabilities in porous media. *Journal of Computational Physics*, 233:373–399, 2013.

[37] G. Scovazzi, A. Gerstenberger, and S. S. Collis. A discontinuous Galerkin method for gravity-driven viscous fingering instabilities in porous media. *Journal of Computational Physics*, 2012.

[38] Shuyu Sun and Jiangguo Liu. A locally conservative finite element method based on piecewise constant enrichment of the continuous galerkin method. *SIAM Journal on Scientific Computing*, 31(4):2528–2548, 2009.

[39] M. F. Wheeler and B. L. Darlow. Interior penalty Galerkin procedures for miscible displacement problems in porous media. *Computational methods in nonlinear mechanics*, pages 485–506, 1980.